

大同新生代火山岩浆的快速喷发

——来自橄榄石地幔捕捞晶的证据

潘荣昊, 朱 磊, 王思佳, 王觊晨, 吴佳怡, 侯 通

(中国地质大学(北京) 地质过程与矿产资源国家重点实验室, 北京 100083)

摘要: 量化研究幔源岩浆从源区迁移至喷发或者侵位的时间尺度, 对理解基性岩浆作用具有重要意义。然而, 对于岩浆的喷发和就位的时间尺度研究仍缺乏有效的约束, 位于我国华北克拉通北部山西大同新生代火山岩群是理想的研究地区。本文以该火山群 ~0.2 Ma 喷发的神泉寺碱性玄武岩为研究对象, 重点研究其中携带的地幔橄榄石捕捞晶来约束喷发前的时间尺度。通过对其开展详细的矿物化学研究, 发现地幔捕捞晶核部的 Fo 值高达 97.7, 为极富镁橄榄石, 结合其极低的 Ca、Mn 和 Ni 含量特征, 认为它们捕获自被交代的地幔橄榄岩。另外, 地幔橄榄石捕捞晶发育明显的 CaO 成分环带, 表明其在地壳岩浆系统内经历了复杂的岩浆演化过程。地幔橄榄石捕捞晶反应边宽度变化很大, 说明它们在源区被捕获时及在运移过程中经过了多次破碎过程。橄榄石捕捞晶最边缘的 Fo 值为 70 左右, 平衡计算表明它们在边部已与主岩浆(碱性玄武岩)达到平衡。Fe-Mg 元素扩散计时结果显示, 橄榄石地幔捕捞晶仅在岩浆中滞留了几个月的时间。对于 40~70 km 的岩石圈地幔厚度来说, 岩浆平均上升速率最快可能超过 500 m/d。

关键词: 大同火山群; 碱性玄武岩; 橄榄石捕捞晶; Fe-Mg 元素扩散计时; 快速喷发; 岩浆上升速率

中图分类号: P588.14⁺5; P588.11

文献标识码: A

文章编号: 1000-6524(2022)03-0519-18

Rapid ascent of basaltic magma beneath the Datong Cenozoic volcanic field: Evidence from mantle olivine xenocrysts

PAN Rong-hao, ZHU Lei, WANG Si-jia, WANG Ji-chen, WU Jia-yi and HOU Tong

(State Key Laboratory of Geological Processes and Mineral Resources, China University of Geosciences, Beijing 100083, China)

Abstract: Quantitatively determining the timescale during mantle-derived magma ascent from the source to eruption or emplacement is essential for the understanding of magmatism, however, the timescales of eruption/emplacement are still poorly constrained. Shanxi Datong Cenozoic volcanic field, north of the North China Craton, is an ideal area for the investigation. In this study, we focused on the mantle olivine xenocrysts entrained in ca. 0.2 Ma Shenzuansi alkali basalt, and its timescale of residence in the host magma prior to eruption. According to mineral chemistry, cores of these mantle olivine xenocrysts have Fo values up to 97.7, which can be defined as extremely magnesian olivine. They are also characterized by the extremely low contents in Ca, Mn and Ni, suggesting they were captured from metasomatized mantle peridotite. Moreover, both of the mantle olivine xenocrysts display complex CaO profiles, attributed to complex magmatic processes in the magma plumbing system. The reaction rim widths of one olivine xenocryst vary significantly, implying it has experienced multiple crack processes when captured or dur-

收稿日期: 2021-04-20; 接受日期: 2022-02-08; 编辑: 尹淑萍

基金项目: 中央高校基本科研业务费(2652018120); 中国地质大学(北京)“求真学人”计划(265QZ201901); 国家自然科学基金优秀青年科学基金(41922012); 中国地质大学(北京)创新创业训练计划(S202111415017)

作者简介: 潘荣昊(1994-), 博士研究生在读, 矿物学、岩石学、矿床学专业, E-mail: 3001190016@cugb.edu.cn; 通讯作者: 侯 通(1984-), 男, 教授, 岩石学专业, 研究方向为岩浆作用与成矿效应, E-mail: thou@cugb.edu.cn。

ing transport. The Fo values of the mantle olivine xenocrysts rims are about 70, indicating they are in diffusion equilibrium with the host magma (alkali basalt) at rims. Timescales obtained by Fe-Mg diffusion chronometry of olivine mantle xenocrysts show that they have only resided in the magma for months. For a lithospheric mantle thickness of 40~70 km, the fastest average ascent rate may exceed 500 m/d.

Key words: Datong volcanic field; alkali basalt; olivine xenocryst; Fe-Mg diffusion chronometry; rapid ascending magma; magma ascent rate

Fund support: The Fundamental Research Funds for the Central Universities(2652018120); China University of Geosciences, Beijing, “Seeking Truth Scholars” Project(265QZ201901); National Natural Science Foundation of China for Excellent Young Scholars(41922012); China University of Geosciences, Beijing, College Student Innovation and Entrepreneurship Training Program(S202111415017)

岩浆岩的形成和演化受到热力学过程和动力学过程的共同控制(Costa *et al.*, 2020)。近年来,实验岩石学方法和岩石、矿物及熔融包裹体分析测试技术的发展,使岩浆演化的热力学模型日臻成熟。这些热力学模型在探究岩浆喷发前存储状态方面(包括岩浆的存储位置、分异过程、脱气作用和岩浆混合等)得到了广泛应用(如 Blundy and Cashman, 2008; Cashman *et al.*, 2017)。然而,绝大多数热力学模型都是基于矿物-熔体平衡来建立的,但是越来越多的研究发现,自然样品中矿物和岩石之间很少能够达到平衡(Pichavant and Macdonald, 2007; Laumonier *et al.*, 2014; Annen *et al.*, 2015; Bergantz *et al.*, 2015; Ganne *et al.*, 2018),因此对岩浆演化过程的研究就不得不考虑其中的动力学过程。作为动力学模型的重要参数,岩浆过程的时间尺度已成为近年火山学研究的热点之一。然而,目前对岩浆分异、存储和混合的持续时间以及晶粥体再活化的作用时间还都缺乏较好的约束(Costa and Dungan, 2005; Chakraborty, 2008, 2010; Cooper and Kent, 2014; Dohmen *et al.*, 2017; Cooper, 2019),甚至对幔源岩浆从地幔迁移至岩浆房或地表平均上升速率的估算结果也存在很大差异(表1)。

研究幔源岩浆从地幔迁移至地表的上升速率非常重要,它可以为浅层岩浆房过程、脱气速率、喷发方式和岩浆储运系统的演化过程提供有效约束(Petrelli and Zellmer, 2020)。目前研究该问题的方法主要有一些流体力学模型(如 Sparks and Walker, 1977; Spera, 1980, 1984, 1987; O’Neill and Spiegelman, 2010)、热动力学实验(如 Hofmann and Magaritz, 1977; Wanamaker *et al.*, 1982, 1990; Ozawa, 1984; Szabó and Bodnar, 1996)和矿物成分环带扩散计时(如 Peslier and Luhr, 2006; Demouchy et

al., 2006; Ruprecht and Plank, 2013; Harangi *et al.*, 2013; Brenna *et al.*, 2018)等(表1)。由于岩浆的运移是一种非线性过程,这些力学模型和热动力学实验的边界条件往往设定过于简单,与实际出入较大,所以估算的最终结果不可避免地存在较大误差(如 Rutherford, 2008; Gonnermann and Manga, 2013; Browne and Szramek, 2015; Rivalta *et al.*, 2015; Petrelli and Zellmer, 2020)。基于矿物成分环带的元素扩散计时可以为岩浆作用的时间尺度提供最直接的约束(Costa *et al.*, 2020),估算结果的误差主要来自于元素扩散系数的测定(Petrelli and Zellmer, 2020)。由于橄榄石在玄武质岩石中普遍发育,且测试技术相对简便,模型涉及的扩散系数已经过大量实验校准(Dohmen and Chakraborty, 2007; Dohmen *et al.*, 2007; Holzapfel *et al.*, 2007),对时间尺度的估算结果相对更为可靠,橄榄石元素扩散计时已在对玄武质岩浆系统岩浆过程的研究中得到广泛应用(Kahl *et al.*, 2011; Hartley *et al.*, 2016; Moussallam *et al.*, 2019; Sundermeyer *et al.*, 2020)。对于研究幔源岩浆从地幔迁移至地表的整个时间尺度,扩散过程必须可以涵盖岩浆运移的整个过程。橄榄石OH、CaO和Fe-Mg扩散计时是研究该问题最常用到的3种方法,然而最近的研究发现,OH扩散主要受到岩浆脱气作用控制,可能只能反映地壳浅部过程(Brenna *et al.*, 2018),因此得到的岩浆平均上升速率往往偏大;CaO在橄榄石中含量很低,需要更高精度的测试方法,它的扩散速率也很慢,且扩散系数受氧逸度等影响很大(Chakraborty, 1997; Coogan *et al.*, 2005),往往难以得到理想的扩散曲线,且模拟结果误差较大。橄榄石Fe-Mg元素扩散可以涵盖岩浆从地幔到地壳的整个过程,但由于它们的扩散速率相对较快,如果幔源岩浆经历

表 1 碱性玄武质和其他幔源岩浆从地幔到喷出地表经历的时间尺度和平均上升速率

Table 1 The timescales and average ascent rates from mantle source to eruption on the surface of alkaline basaltic and other mantle-derived magmas

| 文献 | 岩性 | 方法 | 时间尺度 | 起源深度/km | 平均上升速率/(m·s ⁻¹) | 地壳岩浆房 |
|--------------------------------|-------|-------------------|--------------|-----------|-----------------------------|-------|
| Sparks and Walker(1977) | 玄武岩 | 地幔包体沉降模型 | | | >0.001 | |
| Hofmann and Magaritz(1977) | 碱性玄武岩 | 地幔包体粒间熔体 CaO 扩散实验 | <3 d | 60 | >0.2 | |
| Spera(1980) | 碱性玄武岩 | 地幔包体沉降模型 | | | >0.1 | |
| Wanamaker <i>et al.</i> (1982) | 碱性玄武岩 | 地幔橄榄石裂隙愈合实验 | 3~7 d | 60 | 0.1~0.2 | |
| Spera(1984) | 碱性玄武岩 | 动力学和流体力学模型 | | | 0.01~5 | |
| Ozawa(1984) | 碱性玄武岩 | 地幔尖晶石橄榄石间元素扩散实验 | <1 d | 120 | >1.4 | |
| Spera(1987) | 碱性玄武岩 | 简单裂纹扩展模型 | 8 d | 30 | 0.1 | |
| Wanamaker <i>et al.</i> (1990) | 碱性玄武岩 | 地幔橄榄石裂隙愈合实验 | 80~170 h | 35 | 0.001~0.1 | |
| Szabó and Bodnar(1996) | 碱性玄武岩 | 地幔尖晶石成分环带宽度 | 18 h | 60 | 0.93 | |
| Peslier and Luhr(2006) | 碱性玄武岩 | 地幔橄榄石 HO 扩散计时 | 18~65 h | 34.5~40.4 | 0.2~0.5 | |
| | | 橄榄石、辉石捕捞晶溶解模型 | | 40 | >0.5 | |
| Demouchy <i>et al.</i> (2006) | 碱性玄武岩 | 地幔橄榄石 HO 扩散计时 | 1.9~6.3 h | 60~70 | 3~9 | 无 |
| O'Reilly and Griffin(2011) | 碱性玄武岩 | 综述 | | | 0.2~2 | |
| O'Neill and Spiegelman(2010) | 玄武岩 | 岩脉网络模型 | | | 0.24 | |
| | | 岩墙扩展模型 | | | 0.01~10 | |
| Ruprecht and Plank(2013) | 安山岩 | 地幔橄榄石 NiO 扩散计时 | 0.3~2.2 a | 35 | 0.0006~0.0009 | 有 |
| | | 岩墙扩展模型 | | | 0.0012 | |
| Harangi <i>et al.</i> (2013) | 碱性玄武岩 | 地幔橄榄石 CaO 扩散计时 | 1.3 a | 60~90 | 0.001~0.002 | 无 |
| | | 地幔橄榄石 CaO 扩散计时 | 86.4~115.2 h | 60 | 0.14~0.19 | |
| Jankovics <i>et al.</i> (2013) | 碱性玄武岩 | 裂纹扩展模型 | 0.8~1.6 h | 60 | 4.4~9.2 | 无 |
| | | 地幔包体沉降模型 | 40~66 h | 60 | 0.1~0.41 | |
| | | 地幔橄榄石 CaO 扩散计时 | 86.4 h | 60 | 0.19 | |
| | | 地幔斜方辉石溶解模型 | 86~426 min | 60 | 11.9 | |
| | | 紊流裂纹扩展模型 | 1.7~8.5 h | 50 | 1.6~8.4 | |
| | | 地幔包体沉降模型 | 41~139 h | 50 | 0.1~0.34 | |
| | | 地幔斜方辉石溶解模型 | 20~100 min | 50 | 8.3~41.6 | |
| | | 地幔橄榄石 CaO 扩散计时 | 126 h | 50 | 0.11 | |
| Ray <i>et al.</i> (2016) | 碱性玄武岩 | 综述 | | | 0.001~10 | |
| Hayes <i>et al.</i> (2018) | 玄武岩 | | | | | |
| Brenna <i>et al.</i> (2018) | 碱性玄武岩 | 地幔橄榄石 Fe-Mg 扩散计时 | ~1 m | 27~80 | 0.01~0.03 | 无 |
| | | 地幔橄榄石 HO 扩散计时 | 0.75~12 h | 27~80 | <~10 | |
| Petrelli and Zellmer(2020) | 玄武岩 | 综述 | | | 0.01~25 | |
| 本研究 | 碱性玄武岩 | 地幔橄榄石 Fe-Mg 扩散计时 | 131~263 d | 40~70 | 0.0018~0.0062 | 有 |

了较为复杂的地壳过程, 如存在多级岩浆房、多期岩浆混合、多期结晶等过程, 橄榄石与相对演化的熔体发生长期的相互作用, 其核部成分常常由于扩散再平衡而被改变, 获取更深部岩浆过程的信息就受到了限制, 因此大多数橄榄石 Fe-Mg 扩散的研究也只聚焦于从岩浆房到喷发至地表的浅部过程(Gordychik *et al.*, 2018)。目前采用该方法研究玄武质岩浆从地幔运移至地表整个时间尺度的应用仅有 1 例(Brenna *et al.*, 2018), 因此还需要更多的约束。Brenna 等(2018)对活动大陆边缘单成因火山携带的地幔橄榄石捕捞晶 Fe-Mg 扩散计时的研究结果显示, 即使岩浆可能在地壳岩浆房中停留, 碱性玄武质岩浆上升也可以非常快, 速率可达到 0.01~0.03 m/s。

华北克拉通山西大同盆地东部新生代火山群神泉寺玄武岩中发育有地幔捕捞晶, 这些地幔捕捞晶的核部还保留着地幔信息, 尚未被后期的捕捞晶-熔体相互作用所完全“抹去”, 为研究板内玄武质岩浆作用从地幔上升至地表的整个时间尺度提供了绝佳的机会。本文通过橄榄石 Fe-Mg 元素扩散计时模拟, 得出神泉寺玄武质岩浆从地幔穿越大陆地壳上升至地表只经过了数月的时间。

1 地质概况

华北克拉通(图 1a)是世界上最古老的地质单元之一, 具有约 3.8 Ga 的变质变形历史(Liu *et al.*,

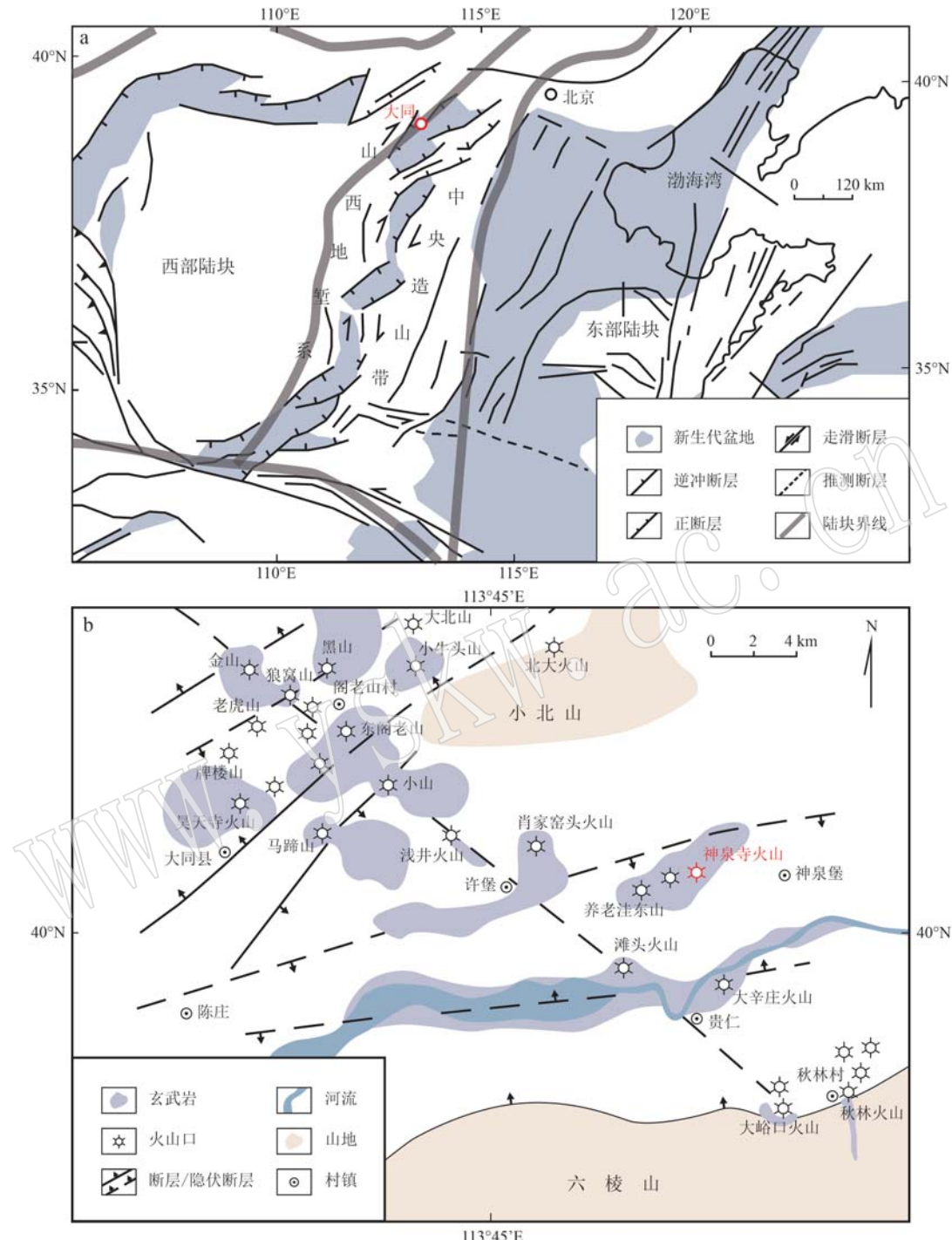


图1 华北克拉通地质构造简图(a, 据Kusky *et al.*, 2007; 陆块界线据Zhao *et al.*, 2001)及大同盆地东部火山群火山分布图(b, 据王乃樑等, 1996)

Fig. 1 Simplified tectonic map of the North China Craton (a, after Kusky *et al.*, 2007; block boundaries are from Zhao *et al.*, 2001) and the distribution of volcanic centers in Datong basin eastern volcanic field (b, after Wang Nailiang *et al.*, 1996)

1992; 万渝生等, 2001, 2009; Wu *et al.*, 2008), 在新太古代晚期(2.5 Ga)完成微陆块拼合和克拉通化(Zhai and Liu, 2003; 万渝生等, 2005; Zhao *et al.*,

2005; Geng *et al.*, 2006; Kusky *et al.*, 2007), 基底主要为英云闪长岩-奥长花岗岩-花岗闪长岩(TTG)片麻岩。而后, 华北克拉通经历了古元古代末期的

造山作用 (Zhao *et al.*, 1999, 2003, 2005, 2010), 并进入长达 10 多亿年的构造寂静期 (翟明国, 2006, 2011)。

中生代以来, 由于受到太平洋板块西向俯冲的影响, 华北克拉通东部陆块发生了大规模的弧岩浆和基底重熔再造 (Zhang *et al.*, 2014; Wu *et al.*, 2019), 伴随构造伸展变形 (Meng, 2003; Liu *et al.*, 2005; Wang *et al.*, 2011)。金伯利岩地幔包体和金刚石包裹体等证据表明, 华北克拉通东部陆块岩石圈厚度在晚中生代时发生明显减薄 (Menzies *et al.*, 1993; Griffin *et al.*, 1998; Chen *et al.*, 2006), 造成目前具有地温梯度高、地表热流值高的特征 (徐义刚, 2006)。与此不同的是, 西部陆块和中央造山带的岩石圈一直较厚, 且岩浆活动仅仅出现在局部地区 (Xu, 2002; Zhang *et al.*, 2003; Xu *et al.*, 2005)。从始新世到渐新世, 由于华北克拉通西南侧受到印度板块东向挤压, 东侧受到太平洋板块西向俯冲的影响, 中央造山带内邻接西部陆块的一侧形成了 S 型的山西地堑系 (Ye *et al.*, 1987; Ren *et al.*, 2002)。山西地堑系从燕山一直延伸到秦岭, 地堑系内分布有一系列地堑盆地, 大同盆地是最北端的一个盆地 (图 1a)。

大同盆地出露地层主要为太古宙片麻岩系, 上覆第四系黄土及河湖相粘土堆积 (裴静娴, 1981)。区内断裂构造十分发育, 主要有桑干河断裂、陈庄-许堡断裂、六棱山前断裂等北东向断裂和许堡-阁老庄断裂等北西向断裂 (张世民等, 1997)。第四纪以来, 受新构造运动的影响, 沿盆地内出现一系列火山喷发和岩浆溢出, 形成大同盆地东部、北部和南部 3 个火山群 (王乃樑等, 1996)。大同盆地东部火山群共计有 30 余座火山 (图 1b), 从岩性上可大致沿陈庄-许堡断裂划分为东区和西区, 东区主要为裂隙式喷发的拉斑玄武岩, 喷发年代始于 0.74 Ma; 西区主要为中心式喷发的碱性玄武岩, 喷发年代始于 0.4 Ma (张彦波, 1986; 陈文寄等, 1992; 樊祺诚等, 1992; 陈孝德等, 2001; Xu *et al.*, 2005; 安卫平等, 2008; 孙嘉祥等, 2020)。前人认为, 大同盆地东部火山群岩性的空间变化, 可能是岩浆来自于不同源区深度导致的 (陈孝德等, 2001; 马金龙等, 2004; Xu *et al.*, 2005)。神泉寺火山 (图 1b) 位于陈庄-许堡断裂之上, 热释光法测得喷发年龄为 0.22 ~ 0.19 Ma (李虎侯等, 1984)。本次研究的样品为陈玲 (2019) 采集的神泉寺熔岩流 SQS-02, 全岩地球化

学成分显示其为碱性玄武岩。

2 岩相学特征

神泉寺玄武岩样品 SQS-02 具灰黑色块状构造、气孔状构造, 气孔约占 20%。斑状结构, 斑晶含量约为 25%, 基质含量约为 55%。斑晶主要有单斜辉石 (10%)、斜长石 (10%) 和橄榄石 (5%)。单斜辉石斑晶常常为自形到半自形短柱状, 有时可见筛状结构 (图 2a), 粒径小于 1 mm; 斜长石斑晶常常呈自形到半自形宽板状, 粒径一般小于 1 mm (图 2b); 橄榄石斑晶常常为自形到半自形粒状, 粒径大多小于 0.5 mm (图 2b)。基质主要为斜长石 (30%)、单斜辉石 (15%) 和橄榄石 (10%) 以及少量铁钛氧化物, 大多呈间粒结构, 即它形的单斜辉石、橄榄石和铁钛氧化物充填于自形的斜长石颗粒之间。

样品薄片中发现两颗橄榄石捕捞晶 OLe1 和 OLe2 (图 2c, 2d)。OLe1 粒径约为 0.4 mm, 它形, 颗粒边部具有明显的成分环带, 然而环带宽度在不同方向上变化很大, 从几个 μm 到 100 μm 不等 (图 2c), 可能最初环带形成之后在岩浆通道内经历了破碎。OLe2 粒径约为 0.5 mm, 半自形, 边部也具有明显的成分环带, 环带宽度分布较为均匀, 约为 100 μm (图 2d)。

3 测试方法

橄榄石捕捞晶的化学成分由电子探针分析 (EMPA) 获得。EMPA 测试在自然资源部第二海洋研究所海底科学重点实验室完成, 测试仪器型号为日本电子 JOEL JXA-8100, 配备 4 道波谱仪 (5B-92U) 和 1 道能谱仪 (Oxford INCA X-sight, 5B-92U, 能量分辨率 133 eV@ MnK α), 测试加速电压为 15 kV, 电流为 300 nA, Si、Ti、Al、Mg、Cr 元素的峰值接收时间为 10 s, Fe 元素为 30 s, Ca、Mn、Ni 元素为 100 s, 背景接收时间为峰值接收时间的一半, 数据通过 ZAF 法进行校正。测试束斑直径为 1 μm , 剖面步长为 5 μm 。测试采用的标样为中国微束分析标准委员会研制的微束分析系列国家标准样品和美国 SPI 公司研制的相关金属和矿物标样, 测试值与标准值的相对误差不超过 3%。橄榄石捕捞晶的高清背散射图片由相同仪器拍摄。

由于橄榄石具有强烈的各向异性, 橄榄石中

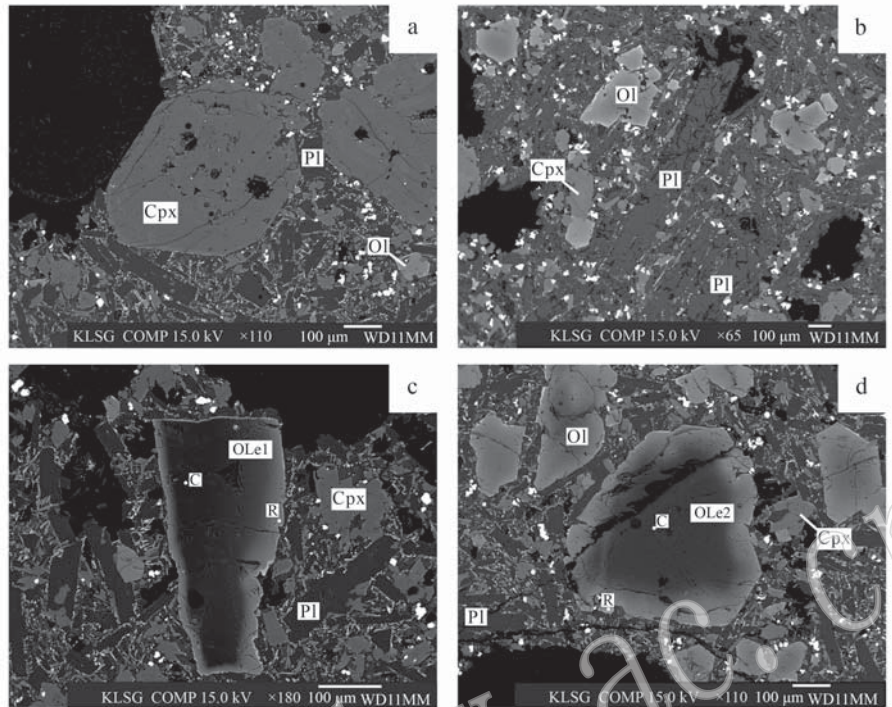


图2 神泉寺玄武岩背散射(BSE)照片

Fig. 2 Back scattered electron (BSE) images of Shenquansi basalt

a—发育筛状结构的单斜辉石斑晶; b—橄榄石和斜长石斑晶; c—橄榄石捕掳晶 OLe1; d—橄榄石捕掳晶 OLe2; Cpx—单斜辉石; Ol—橄榄石; Pl—斜长石; C 和 R 分别为橄榄石捕掳晶核部和边部的探针点位

a—clinopyroxene phenocryst showing sieve texture; b—olivine and plagioclase phenocrysts; c—olivine xenocryst OLe1; d—olivine xenocryst OLe2; Cpx—clinopyroxene; Ol—olivine; Pl—plagioclase; C (core) and R (rim) represent the spots of electron microprobe analysis on olivine xenocrysts

Fe-Mg元素的扩散系数在不同晶轴方向上有明显差异,因此需要准确知道橄榄石的晶格方向(Costa and Chakraborty, 2004; Dohmen *et al.*, 2007; Chakraborty, 2010)。本研究中橄榄石捕掳晶的晶格方向通过电子背散射衍射(EBSD)获得。EBSD测试在中国地质科学院地质研究所大陆构造与动力学重点实验室完成,测试仪器型号为Quanta450,晶体晶格方向相关参数由Aztec软件读取。首先,对电子探针点位(橄榄石核部和边部)附近进行点测试,MAD小于0.5时,读取晶格方向的相关参数。点测试表明橄榄石核部和边部的晶格方向一致,之后进行两点间的线扫描,去除如受裂隙影响的异常点后得出最终的晶格方向。测试剖面的方向与晶格方向的夹角通过软件Stereonet 9.5得到(Allmendinger *et al.*, 2011)。

4 结果与分析

橄榄石捕掳晶 OLe1 和 OLe2 核部最中心的 Fo 值都极高,分别为 97.7 和 94.0(表2、图3),远高于

陈玲(2019)报道的神泉寺玄武岩橄榄石斑晶的核部成分(<84)。橄榄石捕掳晶最边部 Fo 值分别为 69.1 和 68.5,与神泉寺玄武岩橄榄石斑晶的边部成分相似(70~75; 陈玲, 2019)。在 OLe1 中 $Fo \geq 97$ 及 OLe2 中 $Fo \geq 93$ 的核部区域, CaO、MnO 和 NiO 的含量都较低,分别为 0.04%~0.34%、0.05%~0.10% 和 <0.01%;这 3 种元素氧化物的含量在它们 $Fo < 70$ 的边部含量都较高,分别为 0.39%~0.43%、0.43%~0.46% 和 0.09%~0.11%。

橄榄石捕掳晶成分剖面图(图3)显示,从核部到边部, OLe1 和 OLe2 的 Fo 值均逐渐降低,总体呈现轻微的“上凸”状,分别距离边部约 40 μm 和 60 μm 时, Fo 值与橄榄石斑晶核部相当,分别距离边部约 20 μm 和 40 μm 时, Fo 值与橄榄石斑晶边部相当。OLe1 的 MnO 和 NiO 含量从核部到边部逐渐升高,而 CaO 含量先升高,在距离边部约 100 μm 和 80 μm 处出现 2 个峰值,随后降低,至距离边部约 20 μm 处时再次升高。OLe2 的 MnO 含量从核部到边部逐渐升高,而 NiO 含量先升高,至约 40 μm 处

表 2 神泉寺玄武岩橄榄石捕捞晶电子探针分析结果
Table 2 Compositions of olivine xenocrysts in Shenquansi basalt by EMPA

w_B/%

| 样品 | SiO ₂ | TiO ₂ | Al ₂ O ₃ | FeO | MnO | MgO | CaO | Cr ₂ O ₃ | NiO | Total | Fo |
|------|------------------|------------------|--------------------------------|-------|------|-------|------|--------------------------------|------|--------|------|
| 边 | 37.93 | 0.06 | 0.05 | 27.51 | 0.45 | 34.47 | 0.42 | 0.00 | 0.09 | 100.96 | 69.1 |
| | 37.68 | 0.06 | 0.03 | 26.80 | 0.44 | 34.27 | 0.40 | — | 0.09 | 99.78 | 69.5 |
| | 38.17 | 0.03 | 0.05 | 24.70 | 0.39 | 36.69 | 0.36 | 0.01 | 0.09 | 100.48 | 72.6 |
| | 37.96 | 0.05 | 0.05 | 24.39 | 0.38 | 36.32 | 0.37 | 0.01 | 0.09 | 99.61 | 72.6 |
| | 38.10 | 0.02 | 0.04 | 22.71 | 0.35 | 37.45 | 0.39 | 0.01 | 0.08 | 99.14 | 74.6 |
| | 38.62 | 0.02 | 0.04 | 20.56 | 0.31 | 39.23 | 0.43 | 0.01 | 0.08 | 99.29 | 77.3 |
| | 39.10 | 0.01 | 0.04 | 18.17 | 0.25 | 41.10 | 0.47 | 0.01 | 0.07 | 99.21 | 80.1 |
| | 39.22 | 0.01 | 0.04 | 16.14 | 0.23 | 42.46 | 0.52 | 0.01 | 0.06 | 98.67 | 82.4 |
| | 39.68 | 0.03 | 0.04 | 14.32 | 0.20 | 43.79 | 0.58 | 0.02 | 0.05 | 98.69 | 84.5 |
| | 39.83 | 0.01 | 0.04 | 12.93 | 0.18 | 44.84 | 0.60 | — | 0.05 | 98.48 | 86.1 |
| | 39.95 | 0.01 | 0.05 | 11.80 | 0.16 | 45.56 | 0.64 | 0.01 | 0.04 | 98.21 | 87.3 |
| | 40.92 | 0.01 | 0.05 | 10.95 | 0.15 | 47.82 | 0.67 | 0.01 | 0.03 | 100.61 | 88.6 |
| | 41.00 | 0.02 | 0.06 | 10.45 | 0.15 | 48.04 | 0.75 | 0.01 | 0.03 | 100.49 | 89.1 |
| | 41.30 | 0.01 | 0.04 | 9.86 | 0.14 | 48.79 | 0.69 | 0.01 | 0.03 | 100.85 | 89.8 |
| | 41.54 | 0.03 | 0.20 | 9.14 | 0.13 | 49.12 | 0.87 | — | 0.02 | 101.04 | 90.6 |
| OLe1 | 40.83 | 0.02 | 0.34 | 8.45 | 0.12 | 49.79 | 0.88 | 0.00 | 0.02 | 100.45 | 91.3 |
| | 41.49 | 0.01 | 0.05 | 7.88 | 0.11 | 49.61 | 0.85 | 0.00 | 0.02 | 100.01 | 91.8 |
| | 41.09 | 0.01 | 0.07 | 7.01 | 0.11 | 49.98 | 0.79 | — | 0.02 | 99.06 | 92.7 |
| | 41.38 | 0.01 | 0.05 | 6.70 | 0.10 | 51.64 | 0.57 | 0.00 | 0.01 | 100.46 | 93.2 |
| | 41.64 | 0.02 | 0.05 | 6.04 | 0.09 | 52.18 | 0.59 | 0.01 | 0.01 | 100.64 | 93.9 |
| | 41.50 | — | 0.04 | 5.63 | 0.09 | 52.18 | 0.70 | 0.01 | 0.01 | 100.16 | 94.3 |
| | 41.70 | 0.03 | 0.08 | 5.10 | 0.08 | 52.52 | 0.71 | 0.00 | 0.01 | 100.23 | 94.8 |
| | 41.80 | 0.01 | 0.06 | 4.62 | 0.07 | 53.26 | 0.42 | 0.01 | 0.01 | 100.25 | 95.4 |
| | 41.75 | 0.02 | 0.18 | 4.30 | 0.07 | 53.11 | 0.38 | 0.01 | 0.01 | 99.82 | 95.7 |
| | 42.26 | 0.01 | 0.03 | 3.76 | 0.06 | 54.22 | 0.29 | 0.01 | 0.01 | 100.64 | 96.3 |
| | 41.92 | 0.02 | 0.08 | 3.69 | 0.06 | 53.80 | 0.31 | — | 0.01 | 99.88 | 96.3 |
| | 41.78 | 0.02 | 0.22 | 3.51 | 0.07 | 53.77 | 0.28 | 0.12 | 0.01 | 99.77 | 96.5 |
| | 41.59 | 0.01 | 0.05 | 3.20 | 0.06 | 53.65 | 0.32 | — | 0.01 | 98.88 | 96.8 |
| | 42.15 | 0.05 | 0.05 | 3.14 | 0.06 | 54.24 | 0.29 | — | 0.01 | 99.98 | 96.9 |
| | 41.91 | 0.04 | 0.06 | 2.66 | 0.05 | 54.51 | 0.33 | 0.00 | 0.00 | 99.56 | 97.3 |
| | 42.14 | 0.01 | 0.05 | 2.60 | 0.05 | 54.50 | 0.34 | 0.01 | 0.01 | 99.70 | 97.4 |
| | 42.01 | 0.01 | 0.03 | 2.57 | 0.05 | 54.57 | 0.21 | — | 0.01 | 99.46 | 97.4 |
| 核 | 42.15 | — | 0.02 | 2.25 | 0.05 | 54.47 | 0.11 | — | 0.00 | 99.04 | 97.7 |
| 边 | 37.73 | 0.08 | 0.05 | 27.97 | 0.46 | 34.11 | 0.43 | 0.00 | 0.09 | 100.92 | 68.5 |
| | 37.36 | 0.07 | 0.04 | 27.65 | 0.44 | 33.64 | 0.42 | — | 0.10 | 99.73 | 68.4 |
| | 37.44 | 0.06 | 0.04 | 27.29 | 0.45 | 33.99 | 0.40 | — | 0.11 | 99.78 | 68.9 |
| | 37.62 | 0.04 | 0.03 | 26.77 | 0.43 | 34.73 | 0.39 | — | 0.11 | 100.13 | 69.8 |
| | 37.62 | 0.05 | 0.05 | 25.78 | 0.40 | 35.21 | 0.36 | 0.01 | 0.13 | 99.61 | 70.9 |
| | 37.73 | 0.04 | 0.06 | 25.58 | 0.39 | 35.24 | 0.36 | 0.01 | 0.13 | 99.53 | 71.1 |
| | 37.81 | 0.04 | 0.03 | 25.10 | 0.39 | 35.82 | 0.34 | 0.01 | 0.13 | 99.66 | 71.8 |
| | 37.87 | 0.02 | 0.03 | 24.22 | 0.37 | 36.47 | 0.34 | 0.01 | 0.13 | 99.45 | 72.9 |
| OLe2 | 38.14 | 0.03 | 0.04 | 23.19 | 0.34 | 37.27 | 0.34 | 0.03 | 0.14 | 99.51 | 74.1 |
| | 38.47 | 0.02 | 0.04 | 22.07 | 0.32 | 38.31 | 0.36 | 0.02 | 0.12 | 99.72 | 75.6 |
| | 38.77 | 0.01 | 0.04 | 19.55 | 0.27 | 40.07 | 0.41 | 0.01 | 0.12 | 99.25 | 78.5 |
| | 39.09 | 0.03 | 0.07 | 17.57 | 0.24 | 41.47 | 0.50 | 0.02 | 0.10 | 99.08 | 80.8 |
| | 39.83 | 0.03 | 0.04 | 16.18 | 0.22 | 43.57 | 0.53 | 0.03 | 0.08 | 100.51 | 82.8 |
| | 40.21 | 0.01 | 0.06 | 14.70 | 0.21 | 45.09 | 0.59 | 0.00 | 0.05 | 100.92 | 84.5 |
| | 40.38 | 0.01 | 0.02 | 13.90 | 0.20 | 45.29 | 0.45 | 0.00 | 0.05 | 100.31 | 85.3 |
| | 40.83 | 0.00 | 0.02 | 12.52 | 0.17 | 46.35 | 0.48 | — | 0.04 | 100.41 | 86.8 |
| | 40.72 | 0.02 | 0.04 | 12.04 | 0.16 | 46.67 | 0.54 | 0.01 | 0.03 | 100.23 | 87.4 |
| | 40.47 | 0.02 | 0.07 | 11.47 | 0.16 | 47.23 | 0.68 | 0.01 | 0.02 | 100.14 | 88.0 |

续表 1

Continued Table 1

| 样品 | SiO ₂ | TiO ₂ | Al ₂ O ₃ | FeO | MnO | MgO | CaO | Cr ₂ O ₃ | NiO | Total | Fo |
|------|------------------|------------------|--------------------------------|------|------|-------|------|--------------------------------|------|--------|------|
| OLE2 | 40.70 | 0.01 | 0.09 | 9.78 | 0.13 | 49.21 | 0.49 | — | 0.01 | 100.42 | 90.0 |
| | 40.89 | 0.01 | 0.05 | 8.75 | 0.13 | 50.33 | 0.43 | — | 0.01 | 100.59 | 91.1 |
| | 41.18 | 0.01 | 0.02 | 8.06 | 0.12 | 50.67 | 0.31 | 0.01 | 0.01 | 100.38 | 91.8 |
| | 41.18 | 0.02 | 0.02 | 7.55 | 0.11 | 51.19 | 0.27 | 0.00 | 0.01 | 100.34 | 92.4 |
| | 41.40 | 0.00 | 0.02 | 7.21 | 0.11 | 51.51 | 0.20 | 0.01 | 0.01 | 100.47 | 92.7 |
| | 41.45 | — | 0.01 | 7.09 | 0.10 | 51.67 | 0.16 | — | 0.01 | 100.49 | 92.9 |
| | 41.32 | — | 0.03 | 6.91 | 0.10 | 51.59 | 0.13 | 0.01 | 0.00 | 100.10 | 93.0 |
| | 41.36 | — | 0.02 | 6.77 | 0.09 | 51.82 | 0.10 | — | 0.01 | 100.17 | 93.2 |
| | 41.53 | 0.01 | 0.02 | 6.75 | 0.09 | 51.90 | 0.08 | — | 0.01 | 100.37 | 93.2 |
| | 41.52 | 0.00 | 0.02 | 6.60 | 0.10 | 52.14 | 0.06 | 0.01 | 0.00 | 100.45 | 93.4 |
| | 41.38 | — | 0.02 | 6.60 | 0.09 | 51.96 | 0.05 | — | 0.00 | 100.10 | 93.4 |
| | 41.43 | — | 0.01 | 6.49 | 0.09 | 51.91 | 0.06 | 0.01 | 0.00 | 100.02 | 93.4 |
| | 41.51 | 0.01 | 0.01 | 6.49 | 0.09 | 51.89 | 0.04 | 0.02 | 0.01 | 100.06 | 93.4 |
| | 41.49 | 0.00 | 0.01 | 6.39 | 0.09 | 52.13 | 0.04 | 0.01 | 0.00 | 100.16 | 93.6 |
| 核 | 41.56 | 0.00 | 0.01 | 5.94 | 0.08 | 52.05 | 0.04 | 0.00 | 0.00 | 99.67 | 94.0 |

注: —为低于检测限。

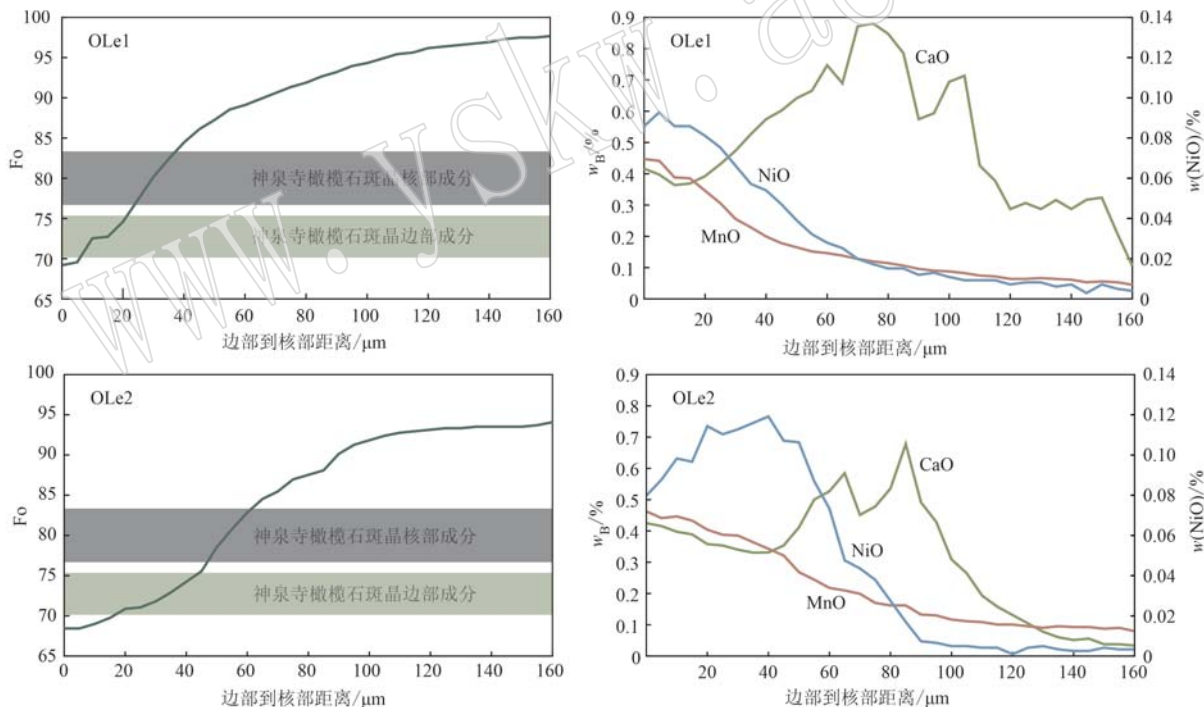


图 3 神泉寺玄武岩橄榄石捕虏晶成分剖面图(橄榄石斑晶数据引自陈玲, 2019)

Fig. 3 Compositional profile of olivine xenocrysts in Shenquansi basalt (data of olivine phenocrysts are from Chen Ling, 2019 for comparison)

时开始降低, 与记录的橄榄石斑晶边部结晶位置一致。与 OLe1 相似, OLe2 的 CaO 含量成分剖面也显示出 2 个峰值, 分别出现在距离边部约 80 μm 和 60 μm 处, 随后 CaO 开始降低, 至 40 μm 处再次升高。

OLE1 和 OLe2 的 CaO 含量成分剖面分别在距离边部约 20 μm 和 40 μm 处弯折, 对应了橄榄石斑晶边部结晶, 而 2 处峰值出现的位置均早于橄榄石斑晶核部的结晶。

5 讨论

5.1 极富镁橄榄石来源

不同来源矿物晶体提取出的时间尺度信息代表着不同岩浆过程的时间跨度, 本文研究的橄榄石捕捞晶核部的 Fo 值远高于同一玄武岩中橄榄石斑晶的 Fo 值, 表明它们是外来的捕捞晶。然而, 这些橄榄石捕捞晶核部的 Fo 值也高于一般地幔橄榄石的 Fo 值(88~93; Plechov *et al.*, 2018), 因此需要首先考虑这些橄榄石是否的确来自于地幔。

橄榄石捕捞晶 OLe1 核部的 Fo 值超过了 97, 分类上可被称为极富镁橄榄石 (extremely magnesian olivine, Fo>96; Plechov *et al.*, 2018)。极富镁橄榄石在全球范围内的火成岩中时有报道, 大致有以下几种成因: ① 黑橄榄石 (black olivine), 常见于火山机构内遭受氧化的岩石中, Fo 值最高可达 99.8 (Sigurdsson and Brown, 1970; Carmichael *et al.*, 1996; Garcia *et al.*, 2000; Blondes *et al.*, 2012; Del Moro *et al.*, 2013); ② 发育于豆荚状铬铁矿矿石或富铬铁矿的岩石中, Fo 值最高可达 97.5 (Xu *et al.*, 2009; Huang *et al.*, 2014; Yang *et al.*, 2015; Xiong *et al.*, 2015; Plechov *et al.*, 2018); ③ 发育于碳酸岩或碳酸盐-硅酸盐火山岩中, Fo 值最高可达 99.5 (Treiman and Essene, 1984; Fulignati *et al.*, 2000; Panina *et al.*, 2003; Guzmics *et al.*, 2011; Plechov *et al.*, 2017); ④ 发育于矽卡岩或硅质大理岩中, Fo 值最高可达 99.8 (Zharikov, 1970; Wenzel *et al.*, 2002; Di Rocco *et al.*, 2012; Nekrylov *et al.*, 2021); ⑤ 发育于被交代的地幔橄榄岩中, Fo 值最高可达 97.8 (Ishimaru and Arai, 2011; Zhang *et al.*, 2017)。

橄榄石被氧化时, Fe^{2+} 会被氧化为 Fe^{3+} , Fe^{3+} 很难存在于橄榄石晶格中而被析出, 因此剩余的橄榄石显示出极高的 Fo 值 (Blondes *et al.*, 2012; Del Moro *et al.*, 2013)。由于氧化析出的含铁矿物不能完全从橄榄石晶体中分离, 这种橄榄石常常发育有赤铁矿等含铁矿物条带, 使它在手标本上看起来发黑, 被称为“黑橄榄石” (Moseley, 1984; Banfield *et al.*, 1990; Deer *et al.*, 1992; Ashworth and Chambers, 2000; Blondes *et al.*, 2012; Plechov *et al.*, 2018)。然而, 本次研究的橄榄石捕捞晶中并没有发育含铁矿物条带, 因此不是结晶后被氧化的产物。

由于橄榄石和铬铁矿发生结晶后 Fe-Mg 再平衡, 蛇绿岩套中的豆荚状铬铁矿矿石或一些富铬铁矿的岩石中的橄榄石便可能产生极高的 Fo 值 (Huang *et al.*, 2014)。然而, 这些极富镁橄榄石有一个显著的特点, 它们的 NiO 含量普遍很高, 一般高于 0.5%, 最高可达约 1.4% (图 4; Xu *et al.*, 2009; Yang *et al.*, 2015; Xiong *et al.*, 2015; Plechov *et al.*, 2018)。然而, 本次研究的橄榄石捕捞晶的高镁核部 NiO 含量极低, 只有 0~0.01%, 与该种情况不符。

当有碳酸盐加入到岩浆过程中时, 如较纯的碳酸岩岩浆或含碳酸盐的硅酸盐岩浆, 就可能会产生极富镁橄榄石 (Treiman and Essene, 1984; Rosatelli *et al.*, 2000; Wenzel *et al.*, 2002; Sobolev *et al.*, 2009, 2015; Guzmics *et al.*, 2011; Plechov *et al.*, 2017), 因为碳酸盐的加入会使岩浆变得更为氧化、且硅活度被降低, 橄榄石固溶体中的铁橄榄石会通过如下两种反应分解: ① $3 \text{Fe}_2\text{SiO}_4$ (铁橄榄石) + O_2 = $2 \text{Fe}_3\text{O}_4$ (磁铁矿) + 3SiO_2 ; ② $4 \text{Fe}_2\text{SiO}_4$ (铁橄榄石) + S_2 = $2 \text{Fe}_3\text{O}_4$ (磁铁矿) + 2FeS (磁黄铁矿) + 4SiO_2 , 从而使得残余的橄榄石 Fo 值升高 (Treiman and Essene, 1984)。然而, 部分碳酸岩中的橄榄石 MnO 含量非常高, 高于 1%, 甚至高于 2% (图 4; Treiman and Essene, 1984; Guzmics *et al.*, 2011), 与我们的测试结果不符; 另外一部分橄榄石也显示出低 CaO、MnO、NiO 的特征 (Rosatelli *et al.*, 2000; Yao *et al.*, 2021), 然而这些橄榄石常常在岩相上与碳酸盐熔体或矿物伴生, 该现象在神泉寺玄武岩中并未观察到。

镁矽卡岩或硅质大理岩中的极富镁橄榄石几乎不含 NiO 和 Cr_2O_3 , 但它们的 CaO 和 MnO 含量变化范围很宽, 分别为 0.01%~0.26 和 0.02%~0.53% (Nekrylov *et al.*, 2021)。尽管有部分镁矽卡岩或硅质大理岩中极富镁橄榄石的成分与本次研究的橄榄石捕捞晶核部成分非常相似 (Wenzel *et al.*, 2002; Di Rocco *et al.*, 2012; Nekrylov *et al.*, 2021), 但是考虑到研究区内未见出露碳酸盐沉积地层, 而且区内大断裂和次级断裂皆为正断层, 缺乏逆冲断层 (王乃樑等, 1996), 深部也不会有未出露的碳酸盐地层, 因此该种成因模式似乎也不太可能。

极富镁橄榄石可发育在被交代的地幔橄榄岩包体中, 而且含有极富镁橄榄石的橄榄岩包体在同属华北克拉通中央造山带、大同东南约 120 km 处的中

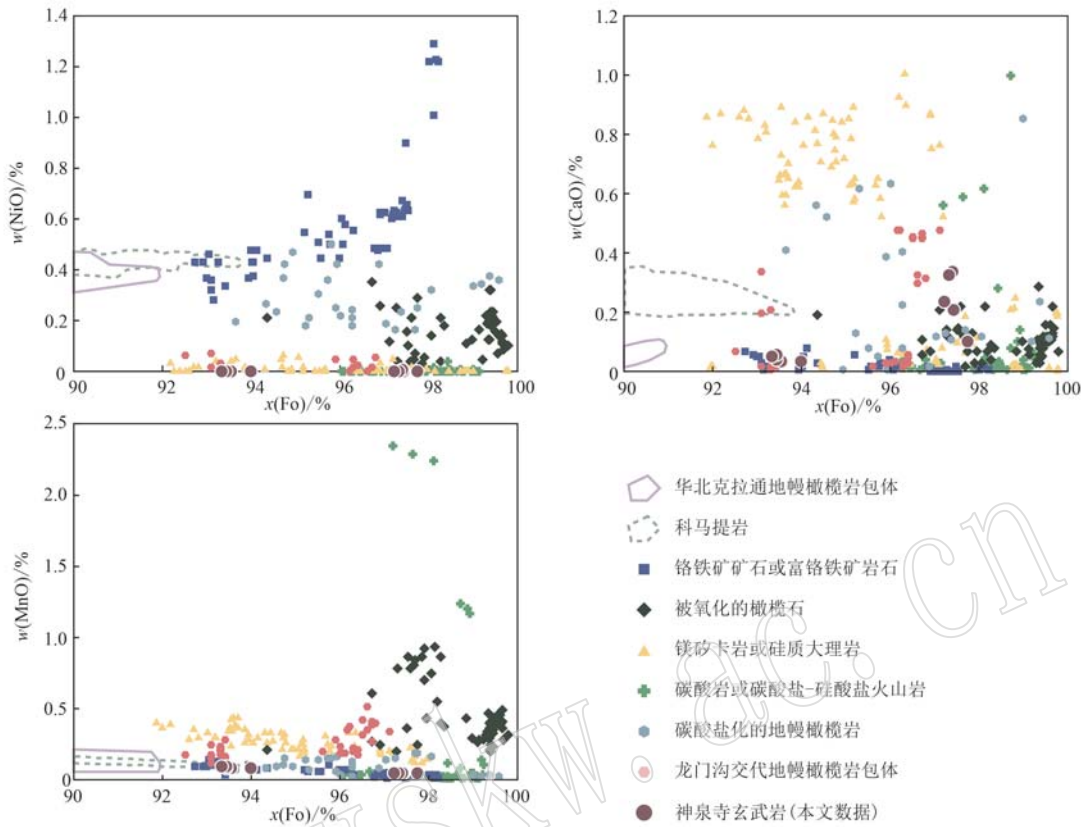


图4 神泉寺玄武岩橄榄石捕捞晶成分与不同构造环境下橄榄石成分的对比

Fig. 4 Compositions of olivine xenocrysts in Shenquansi basalt, compared with olivine from various tectonic environments

华北克拉通地幔橄榄岩包体数据引自 Liu et al. (2010, 2011), Tang et al. (2007, 2014), Zhao et al. (2015), Hu et al. (2019); 科马提岩数据引自 Sobolev et al. (2007); 铬铁矿矿石或富铬铁矿岩石数据引自 Mondal et al. (2006), Yang et al. (2015), Xiong et al. (2015), Plechov et al. (2018); 被氧化的橄榄石数据引自 Carmichael et al. (1996), Garcia et al. (2000), Cortés et al. (2006), Blondes et al. (2012), Del Moro et al. (2013), Ejima et al. (2017); 锰矽卡岩或硅质大理岩数据引自 Di Rocco et al. (2012), Plechov et al. (2018), Nekrylov et al. (2021); 碳酸岩或碳酸盐-硅酸盐火山岩数据引自 Treiman and Essene (1984), Rosatelli et al. (2000), Wenzel et al. (2002), Panina et al. (2003), Guzmics et al. (2011), Yao et al. (2021); 碳酸盐化的地幔橄榄岩数据引自 Gervasoni et al. (2017), He et al. (2020), 龙门沟交代地幔橄榄岩包体数据引自 Zhang et al. (2017)

data for mantle peridotite xenoliths in the North China Craton are from Liu et al. (2010, 2011), Tang et al. (2007, 2014), Zhao et al. (2015) and Hu et al. (2019); data for komatiites are from Sobolev et al. (2007); data for chromitites and chromite-rich rocks are from Mondal et al. (2006), Yang et al. (2015), Xiong et al. (2015) and Plechov et al. (2018); data for oxidized olivines are from Carmichael et al. (1996), Garcia et al. (2000), Cortés et al. (2006), Blondes et al. (2012), Del Moro et al. (2013) and Ejima et al. (2017); data for magnesian skarns and silicate marbles are from Di Rocco et al. (2012), Plechov et al. (2018) and Nekrylov et al. (2021); data for carbonatites and carbonate-silicate rocks are from Treiman and Essene (1984), Rosatelli et al. (2000), Wenzel et al. (2002), Panina et al. (2003), Guzmics et al. (2011) and Yao et al. (2021); data for carbonate metasomatic mantle xenoliths are from Gervasoni et al. (2017) and He et al. (2020); data for Longmengou metasomatic mantle peridotite xenoliths are from Zhang et al. (2017)

生代龙门沟橄榄辉绿岩中也有报道,这些橄榄石(Fo 值最高达97.8)也表现出低 CaO (<0.48%)、低 NiO (<0.08%,大多低于检测限)、低 MnO (<0.52%)的特征(Zhang et al., 2017),本次研究中的橄榄石捕捞晶核部成分与之相符。Zhang等(2017)认为,这些橄榄岩包体代表了经历过大量岩浆抽取的极度亏损的太古宙地幔,橄榄石高 Fo 值低 NiO 含量的特

征是地幔随后与一种高 Mg 、 Ca 低 Ni 的熔体反应导致的,这种熔体被认为是中央造山带被剥离的古元古代山根部分熔融产生的(Xu et al., 2010a, 2010b),因此,本次研究中的橄榄石捕捞晶应该为地幔捕捞晶。

5.2 岩浆平均上升速率

除晶格方向外,橄榄石 $\text{Fe}-\text{Mg}$ 元素的扩散速率还

受温度、压力和氧逸度的影响(Costa and Chakraborty, 2004; Dohmen *et al.*, 2007; Chakraborty, 2010)。对于温度,本文采用陈玲(2019)通过橄榄石斑晶-熔体平衡计算得出的神泉寺岩浆喷发前温度,即裹挟这些橄榄石捕捞晶的岩浆的温度,平均约为1 200℃。对于压力,本文采用陈玲(2019)通过单斜辉石斑晶-熔体平衡计算得出的神泉寺岩浆喷发前的压力,平均约为700 MPa,该压力值也近似大同地区的平均中地壳压力(莫霍面深度约为40 km; He *et al.*, 2014; Zhang *et al.*, 2016)。对于氧逸度,神泉寺玄武岩中单斜辉石斑晶的 $\text{Fe}^{3+}/\text{Fe}^{2+}$ 值大多为0.2~0.6(陈玲, 2019),根据单斜辉石氧逸度计(Cortés *et al.*, 2006)计算得出神泉寺玄武质岩浆的氧逸度平均约为QFM+2(QFM为石英-铁橄榄石-磁铁矿氧逸度缓冲剂),该值也接近大同以北约100 km处的汉诺坝新生代玄武岩岩浆的氧逸度(QFM+2.77;张毅刚等,1994)。最终,橄榄石捕捞晶Fe-Mg元素扩散时间尺度模拟通过DIPRA(Diffusion Process Analysis)软件(Girona and Costa, 2013)得出,OLe1的扩散时间为131 d, OLe2的扩散时间为263 d(图5)。如前文所述,两颗橄榄石捕捞晶皆来自于岩石圈地幔,Xu等(2005)根据玄武岩稀土元素特征和Sr-Nd同位素特征推测大同拉斑玄武岩源区深度约

为65 km,而碱性玄武岩的源区深度应该比之要深,大概为75 km,甚至超过80 km(Xu *et al.*, 2005)。而大地电磁深反射剖面表明,大同岩石圈地幔深度约为40~70 km(Guo *et al.*, 2016),因此,神泉寺碱性玄武岩的源区深度很可能位于岩石圈地幔的最深处(~70 km),橄榄石地幔捕捞晶在岩浆上升途中被捕获。假设两种最极端的情况,两颗橄榄石在岩石圈地幔最深处(70 km)或最浅处(40 km)被捕获,则可以得出岩浆平均上升速率的范围为0.001 8~0.006 2 m/s(相当于152~534 m/d),与前人估算的碱性玄武质岩浆>0.001 m/s的平均上升速率一致(表1; Sparks and Walker, 1977; Wanamaker *et al.*, 1990; Harangi *et al.*, 2013; Hayes *et al.*, 2018)。

5.3 岩浆储运系统

这两颗橄榄石捕捞晶边部具有相似的Fo值(~70),且与橄榄石斑晶边部的Fo值相似(图3),表明它们在主岩浆中滞留的时间都已足够长,虽然核部成分仍然保留着地幔信息,但边部成分都已与主岩浆达到平衡,因此它们不同的扩散计时时间表明OLe2比OLe1更早与岩浆发生相互作用。而不同滞留时间的地幔捕捞晶被捕获至同一股岩浆中,它们有可能经历了以下两种过程:①两颗捕捞晶来自不

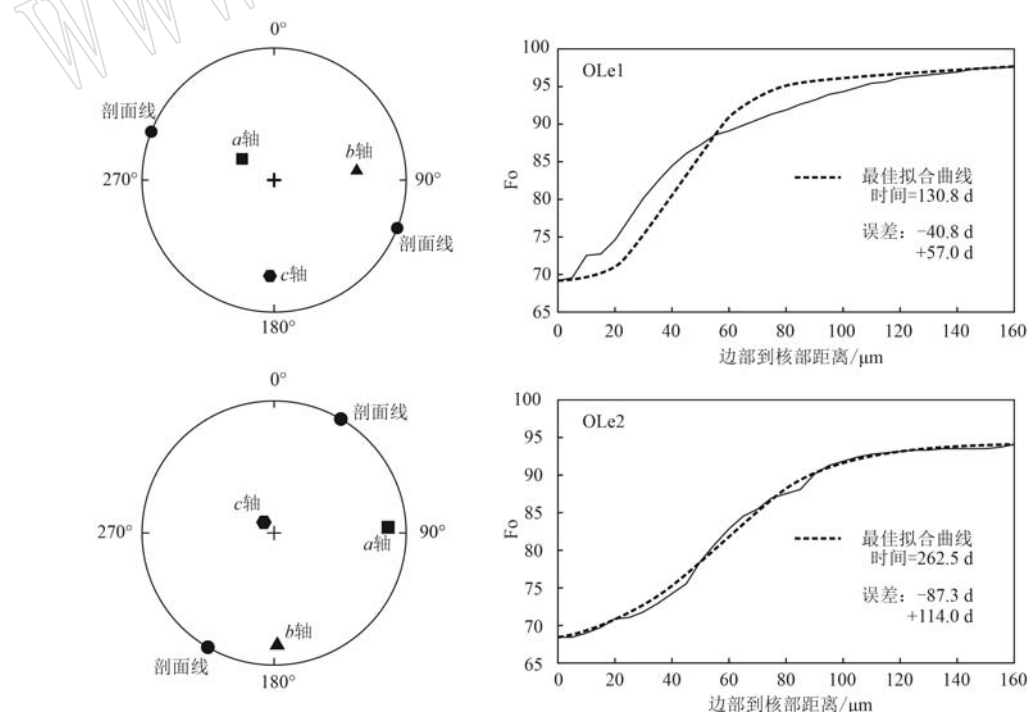


图5 神泉寺橄榄石捕捞晶晶格方向极射赤平投影图、Fo值成分剖面及Fe-Mg元素扩散模拟结果

Fig. 5 Crystal plane equal angle projections, Fo profiles and Fe-Mg diffusion modelling results of the Shenquansi olivine xenocrysts

同的地幔深度, OLe2 比 OLe1 来自于岩石圈地幔的更深处, 岩浆首先捕获 OLe2, 在上升过程中又捕获了 OLe1, 二者一同被携带喷发出地表; ② 两颗捕捞晶来自相同或不同的地幔深度, OLe1 和 OLe2 被不同岩浆捕获, OLe2 较早被捕获, 但相对于 OLe1, 捕获 OLe2 的岩浆随后在地壳内经历了更为复杂的岩浆过程, 导致停留时间更长, 最终与捕获 OLe1 的岩浆混合, 喷发出地表。

笔者认为它们更可能经历了过程①，因为这两颗橄榄石捕捞晶 CaO 含量成分剖面显示出相似的特征，都表现为从核部到边部先上升，形成两个峰再降低，临近边部时再略微上升的趋势（图 3）。当橄榄石先与富 CaO 熔体接触一定时间再与贫 CaO 熔体接触时，橄榄石的成分剖面上便会出现一个峰（Lynn *et al.*, 2017; Brenna *et al.*, 2018），由于 CaO 在橄榄石中的扩散速度相对较慢（Chakraborty, 1997; Coogan *et al.*, 2005），这个峰便不会因为扩散作用而被“抹掉”。因此，这两颗橄榄石捕捞晶相似的 CaO 含量成分剖面特征表明它们都经历了相似的岩浆混合过程。陈玲（2019）通过斑晶矿物温压计计算发现，压力结果集中在 620~840 MPa，说明神泉寺火山下部约 21~27 km 深处存在地壳岩浆房。这两个峰都出现在橄榄石斑晶结晶之前，因此岩浆混合很可能在岩石圈地幔或下地壳就已经发生了。

本文估算的岩浆平均上升速率虽然与前人一致，但相对于许多碱性玄武质岩浆系统，本文估算的晶体滞留时间偏长、岩浆的平均上升速率偏慢（表1）。同时，注意到捕捞晶 OLe1 背散射图显示出晶体四周的反应边宽度有明显差异（图 2c），很可能是经过了多次破碎的结果。扩散作用会产生分梯度，随着扩散时间变长，扩散距离变长，反应边变宽（Klügel, 1998；Costa *et al.*, 2020）。而 OLe1 只有右侧发育较宽的反应边，说明晶体在这一侧的扩散作用时间较长；其他方向反应边相对较窄，说明晶体在这些地方破碎不久，扩散作用时间短（Klügel, 1998）。因此，偏长的晶体滞留时间很可能反映了这两颗地幔橄榄石在源区就已经和岩浆相互作用过一段时间，然后才从地幔橄榄岩上脱离，再随岩浆上升。

综上所述,得出神泉寺火山最有可能的岩浆储运系统模式及橄榄石捕掳晶复杂环带形成过程(图6):①岩浆在接近70 km深的岩石圈地幔较深处持续产生,冲刷地幔橄榄岩,与地幔橄榄石相互作用形成扩散环带,在进一步冲刷下,地幔橄榄石破碎,

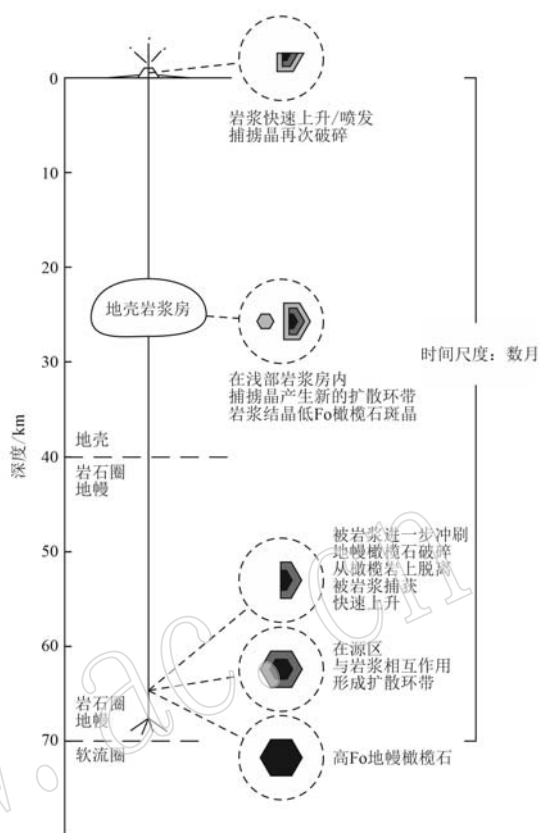


图 6 神泉寺火山岩浆储运系统简图及橄榄石捕掳晶复杂环带形成过程

Fig. 6 Schematic model of the magma plumbing system beneath Shenquansi volcano, and the forming process of the complex zonations of the olivine xenocysts

从橄榄岩上脱落，被岩浆捕获快速上升；② 岩浆在地壳岩浆房中停留演化，橄榄石捕捞晶产生新的扩散环带，晶体破碎处环带较窄，未破碎处环带较宽；岩浆在岩浆房中开始结晶橄榄石斑晶，橄榄石斑晶边部成分与捕捞晶边部成分相似；③ 可能由于深部岩浆补充，岩浆房内的岩浆再次快速上升并喷发，在此过程中橄榄石捕捞晶再次破碎，形成晶体四周环带宽度具有明显差异的复杂环带。

6 结论

- (1) 大同火山群神泉寺碱性玄武岩中发育橄榄石捕捞晶，它们核部的 Fo 值高达 97，为极富镁橄榄石，电子探针成分特征表明它们来自于被交代的地幔。边部 Fo 值均与橄榄石斑晶边部成分相似，表明已与主岩浆发生充分的 Fe-Mg 元素扩散，达到平衡。

(2) Fe-Mg 元素扩散计时显示，岩浆从岩石圈

地幔上升至地表最短仅用 131 d, 最长需要 263 d, 对应岩浆上升速率为 0.001 8~0.006 2 m/s(相当于 152~534 m/d)。

(3) 偏长的晶体滞留时间很可能反映了地幔橄榄石在源区就已经和岩浆相互作用过一段时间, 然后才从地幔橄榄岩上脱离, 再随岩浆上升。橄榄石捕捞晶在不同时期发生破碎, 产生不同宽度的反应边。

致谢 感谢两位匿名审稿人提出的宝贵建议, 也感谢期刊编辑的辛苦工作。感谢自然资源部第二海洋研究所海底科学重点实验室的朱继浩副研究员和鲁江姑博士在电子探针测试过程中提供的帮助, 感谢中国地质科学院地质研究所大陆构造与动力学重点实验室梁风华副研究员和王晓敏技术员在电子背散射衍射测试过程中提供的帮助, 感谢中国地质大学(北京)陈玲硕士对样品的前期处理。

References

- Allmendinger R W, Cardozo N and Fisher D M. 2011. Structural Geology Algorithms: Vectors and Tensors [M]. Cambridge University Press.
- An Weiping and Su Zongzheng. 2008. Landform of volcanoes in Datong of Shanxi [J]. Earthquake Research in Shanxi, 1: 1~5 (in Chinese with English abstract).
- Annen C, Blundy J D, Leuthold J, et al. 2015. Construction and evolution of igneous bodies: Towards an integrated perspective of crustal magmatism [J]. *Lithos*, 230: 206~221.
- Ashworth J R and Chambers A D. 2000. Symplectic reaction in olivine and the controls of intergrowth spacing in symplectites [J]. *Journal of Petrology*, 41(2): 285~304.
- Banfield J F, Veblen D R and Jones B F. 1990. Transmission electron microscopy of subsolidus oxidation and weathering of olivine [J]. *Contributions to Mineralogy and Petrology*, 106(1): 110~123.
- Bergantz G W, Schleicher J M and Burgisser A. 2015. Open-system dynamics and mixing in magma mushes [J]. *Nature Geoscience*, 8(10): 793~796.
- Blondel M S, Brandon M T, Reiners P W, et al. 2012. Generation of forsteritic olivine (Fo 99.8) by subsolidus oxidation in basaltic flows [J]. *Journal of Petrology*, 53(5): 971~984.
- Blundy J and Cashman K. 2008. Petrologic reconstruction of magmatic system variables and processes [J]. *Reviews in Mineralogy and Geochemistry*, 69(1): 179~239.
- Brenna M, Cronin S J, Smith I E, et al. 2018. Olivine xenocryst diffusion reveals rapid monogenetic basaltic magma ascent following complex storage at Pupuke Maar, Auckland Volcanic Field, New Zealand [J]. *Earth and Planetary Science Letters*, 499: 13~22.
- Browne B and Szramek L. 2015. Rates of magma ascent and storage [A]. Sigurdsson H. *The Encyclopedia of Volcanoes* [C]. Elsevier, 203~214.
- Carmichael I S E, Lange R A and Luhr J F. 1996. Quaternary minettes and associated volcanic rocks of Mascota, western Mexico: A consequence of plate extension above a subduction modified mantle wedge [J]. *Contributions to Mineralogy and Petrology*, 124(3~4): 302~333.
- Cashman K V, Sparks R S J and Blundy J D. 2017. Vertically extensive and unstable magmatic systems: A unified view of igneous processes [J]. *Science*, 355(6331): eaag3055.
- Chakraborty S. 1997. Rates and mechanisms of Fe-Mg interdiffusion in olivine at 980~1 300°C [J]. *Journal of Geophysical Research: Solid Earth*, 102(B6): 12 317~12 331.
- Chakraborty S. 2008. Diffusion in solid silicates: A tool to track timescales of processes comes of age [J]. *Annual Review of Earth and Planetary Science*, 36: 153~190.
- Chakraborty S. 2010. Diffusion coefficients in olivine, wadsleyite and ringwoodite [J]. *Reviews in Mineralogy and Geochemistry*, 72(1): 603~639.
- Chen Ling. 2019. Study on the Pre-Eruption State of Cenozoic Volcanic Group Alkaline Basalt in Datong, Shanxi [D]. Beijing: China University of Geosciences (Beijing) (in Chinese with English abstract).
- Chen L, Zheng T Y and Xu W W. 2006. A thinned lithospheric image of the Tanlu Fault Zone, eastern China: Constructed from wave equation based receiver function migration [J]. *Journal of Geophysical Research: Solid Earth*, 111(B09312): 1~15.
- Chen Wenji, Li Daming, Dai Tongmo, et al. 1992. The K-Ar age and excess Ar of Quaternary basalt in Datong [A]. Liu Ruoxin. *The Age and Geochemistry of Cenozoic Volcanic Rock in China* [C]. Beijing: Seismology Press Beijing, 81~92 (in Chinese).
- Chen Xiaode, Shi Lanbin and Lin Chuanyong. 2001. A research on Quaternary volcanism in north China [J]. *Seismology and Geology*, 23(4): 564~573 (in Chinese with English abstract).
- Coogan L A, Hain A, Stahl S, et al. 2005. Experimental determination of the diffusion coefficient for calcium in olivine between 900°C and 1 500°C [J]. *Geochimica et Cosmochimica Acta*, 69(14): 3 683~3 694.
- Cooper K M. 2019. Timescales and temperatures of crystal storage in magma reservoirs: Implications for magma reservoir dynamics [J]. *Philosophical Transactions of the Royal Society A*, 377 (2 139): 20180009.
- Cooper K M and Kent A J. 2014. Rapid remobilization of magmatic crystals kept in cold storage [J]. *Nature*, 506(7 489): 480~483.
- Cortés J A, Wilson M, Condliffe E, et al. 2006. The occurrence of forsterite and highly oxidizing conditions in basaltic lavas from Stromboli volcano, Italy [J]. *Journal of Petrology*, 47(7): 1 345~1 373.

- Costa F and Chakraborty S. 2004. Decadal time gaps between mafic intrusion and silicic eruption obtained from chemical zoning patterns in olivine [J]. *Earth and Planetary Science Letters*, 227(3~4): 517~530.
- Costa F and Dungan M. 2005. Short time scales of magmatic assimilation from diffusion modeling of multiple elements in olivine[J]. *Geology*, 33(10): 837~840.
- Costa F, Shea T and Ubide T. 2020. Diffusion chronometry and the timescales of magmatic processes[J]. *Nature Reviews Earth & Environment*, 1: 201~214.
- Deer W A, Howie R A and Zussman J. 1992. *An Introduction to the Rock-Forming Minerals* [M]. Essex, England: Longman Scientific and Technology.
- Del Moro S, Renzulli A, Landi P, et al. 2013. Unusual lapilli tuff ejecta erupted at Stromboli during the 15 March 2007 explosion shed light on the nature and thermal state of rocks forming the crater system of the volcano[J]. *Journal of Volcanology and Geothermal Research*, 254: 37~52.
- Demouchy S, Jacobsen S D, Gaillard F, et al. 2006. Rapid magma ascent recorded by water diffusion profiles in mantle olivine[J]. *Geology*, 34(6): 429~432.
- Di Rocco T, Freda C, Gaeta M, et al. 2012. Magma chambers emplaced in carbonate substrate: Petrogenesis of skarn and cumulate rocks and implications for CO₂ degassing in volcanic areas[J]. *Journal of Petrology*, 53(11): 2 307~2 332.
- Dohmen R, Becker H W and Chakraborty S. 2007. Fe-Mg diffusion in olivine I: Experimental determination between 700 and 1 200°C as a function of composition, crystal orientation and oxygen fugacity[J]. *Physics and Chemistry of Minerals*, 34(6): 389~407.
- Dohmen R and Chakraborty S. 2007. Fe-Mg diffusion in olivine II: Point defect chemistry, change of diffusion mechanisms and a model for calculation of diffusion coefficients in natural olivine[J]. *Physics and Chemistry of Minerals*, 34(6): 409~430.
- Dohmen R, Faak K and Blundy J D. 2017. Chronometry and speedometry of magmatic processes using chemical diffusion in olivine, plagioclase and pyroxenes [J]. *Reviews in Mineralogy and Geochemistry*, 83(1): 535~575.
- Ejima T, Yoneda M, Akasaka M, et al. 2017. Precipitates within olivine phenocrysts in oxidized andesitic scoria from Kasayama volcano, Hagi, Japan [J]. *Journal of Mineralogical and Petrological Sciences*, 112(3): 116~126.
- Fan Qicheng, Chen Wenji, Hurford A J, et al. 1992. The major and trace element chemistry of Quaternary basalt in Datong [A]. Liu Ruoxin. *The Age and Geochemistry of Cenozoic Volcanic Rock in China* [C]. Beijing: Seismology Press, 93~100 (in Chinese).
- Fulignati P, Marianelli P, Santacroce R, et al. 2000. The skarn shell of the 1944 Vesuvius magma chamber: Genesis and PTX conditions from melt and fluid inclusion data[J]. *European Journal of Mineralogy*, 12(5): 1 025~1 039.
- Ganne J, Bachmann O and Feng X. 2018. Deep into magma plumbing systems: Interrogating the crystal cargo of volcanic deposits [J]. *Geology*, 46(5): 415~418.
- Garcia M O, Pietruszka A J, Rhodes J M, et al. 2000. Magmatic processes during the prolonged Pu'u'O'o eruption of Kilauea Volcano, Hawaii[J]. *Journal of Petrology*, 41(7): 967~990.
- Geng Y, Liu F and Yang C. 2006. Magmatic event at the end of the Archean in eastern Hebei Province and its geological implication[J]. *Acta Geologica Sinica (English Edition)*, 80(6): 819~833.
- Gervasoni F, Klemme S, Rohrbach A, et al. 2017. Experimental constraints on mantle metasomatism caused by silicate and carbonate melts[J]. *Lithos*, 282: 173~186.
- Girona T and Costa F. 2013. DIPRA: A user-friendly program to model multi-element diffusion in olivine with applications to timescales of magmatic processes[J]. *Geochemistry, Geophysics, Geosystems*, 14(2): 422~431.
- Gonnermann H M and Manga M. 2013. Dynamics of magma ascent in the volcanic conduit[A]. Fagents S A, Gregg T K P and Lopes R M C. *Modeling Volcanic Processes: The physics and mathematics of volcanism* [C]. Cambridge University Press, 55~84.
- Gordyechik B, Churikova T, Kronz A, et al. 2018. Growth of, and diffusion in, olivine in ultra-fast ascending basalt magmas from Shiveluch volcano[J]. *Scientific Reports*, 8(1): 1~15.
- Griffin W L, Andi Z, O'reilly S Y, et al. 1998. Phanerozoic evolution of the lithosphere beneath the Sino-Korean Craton[J]. *Mantle Dynamics and Plate Interactions in East Asia*, 27: 107~126.
- Guo Z, Afonso J C, Qashqai M T, et al. 2016. Thermochemical structure of the North China Craton from multi-observable probabilistic inversion: Extent and causes of cratonic lithosphere modification [J]. *Gondwana Research*, 37: 252~265.
- Guzmics T, Mitchell R H, Szabó C, et al. 2011. Carbonatite melt inclusions in coexisting magnetite, apatite and monticellite in Kerimasi calciocarbonatite, Tanzania: Melt evolution and petrogenesis [J]. *Contributions to Mineralogy and Petrology*, 161(2): 177~196.
- Harangi S, Sági T, Seghedi I, et al. 2013. Origin of basaltic magmas of Perşani volcanic field, Romania: A combined whole rock and mineral scale investigation[J]. *Lithos*, 180: 43~57.
- Hartley M E, Morgan D J, MacLennan J, et al. 2016. Tracking timescales of short-term precursors to large basaltic fissure eruptions through Fe-Mg diffusion in olivine[J]. *Earth and Planetary Science Letters*, 439: 58~70.
- Hayes J, Tsang S, Fitzgerald R H, et al. 2018. The DEVORA Scenario-

- os: Multi-hazard Eruption Scenarios for the Auckland Volcanic Field [M]. GNS Science: 1~138.
- He D, Liu Y, Chen C, et al. 2020. Oxidation of the mantle caused by sediment recycling may contribute to the formation of iron-rich mantle melts[J]. *Science Bulletin*, 65(7): 519~521.
- He R, Shang X, Yu C, et al. 2014. A unified map of Moho depth and Vp/Vs ratio of continental China by receiver function analysis[J]. *Geophysical Journal International*, 199(3): 1 910~1 918.
- Hofmann A W and Magaritz M. 1977. Diffusion of Ca, Sr, Ba, and Co in a basalt melt: Implications for the geochemistry of the mantle[J]. *Journal of Geophysical Research*, 82(33): 5 432~5 440.
- Holzapfel C, Chakraborty S, Rubie D C, et al. 2007. Effect of pressure on Fe-Mg, Ni and Mn diffusion in $(Fe_xMg_{1-x})_2SiO_4$ olivine[J]. *Physics of the Earth and Planetary Interiors*, 162(3~4): 186~198.
- Hu J, Jiang N, Carlson R W, et al. 2019. Metasomatism of the crust-mantle boundary by melts derived from subducted sedimentary carbonates and silicates[J]. *Geochimica et Cosmochimica Acta*, 260: 311~328.
- Huang M, Yang J, Powell R, et al. 2014. High-pressure metamorphism of serpentinitized chromitite at Luobusha (southern Tibet)[J]. *American Journal of Science*, 314(1): 400~433.
- Ishimaru S and Arai S. 2011. Peculiar Mg-Ca-Si metasomatism along a shear zone within the mantle wedge: Inference from fine-grained xenoliths from Avacha volcano, Kamchatka[J]. *Contributions to Mineralogy and Petrology*, 161(5): 703~720.
- Jankovics M É, Dobosi G, Embey-Isztin A, et al. 2013. Origin and ascent history of unusually crystal-rich alkaline basaltic magmas from the western Pannonian Basin[J]. *Bulletin of Volcanology*, 75(9): 1~23.
- Kahl M, Chakraborty S, Costa F, et al. 2011. Dynamic plumbing system beneath volcanoes revealed by kinetic modeling, and the connection to monitoring data: An example from Mt. Etna[J]. *Earth and Planetary Science Letters*, 308(1~2): 11~22.
- Klügel A. 1998. Reactions between mantle xenoliths and host magma beneath La Palma (Canary Islands): Constraints on magma ascent rates and crustal reservoirs[J]. *Contributions to Mineralogy and Petrology*, 131(2): 237~257.
- Kusky T, Windley B F and Zhai M G. 2007. Tectonic evolution of the North China Block: From orogen to craton to orogen[J]. *Geological Society, London, Special Publications*, 280(1): 1~34.
- Laumonier M, Scaillet B, Pichavant M, et al. 2014. On the conditions of magma mixing and its bearing on andesite production in the crust[J]. *Nature Communications*, 5(1): 1~12.
- Li Huhou and Sun Jianzhong. 1984. The age of Datong volcanic activity studied by thermoluminescence method[J]. *Science in China Series B—Chemistry, Biological, Agricultural, Medical & Earth Sciences*, 14(7): 637~644 (in Chinese).
- Liu D Y, Nutman A P, Compston W, et al. 1992. Remnants of $\geq 3\ 800$ Ma crust in the Chinese part of the Sino-Korean craton[J]. *Geology*, 20(4): 339~342.
- Liu J, Davis G A, Lin Z, et al. 2005. The Liaonan metamorphic core complex, Southeastern Liaoning Province, North China: A likely contributor to Cretaceous rotation of Eastern Liaoning, Korea and contiguous areas[J]. *Tectonophysics*, 407(1~2): 65~80.
- Liu J, Rudnick R L, Walker R J, et al. 2010. Processes controlling highly siderophile element fractionations in xenolithic peridotites and their influence on Os isotopes[J]. *Earth and Planetary Science Letters*, 297(1~2): 287~297.
- Liu J, Rudnick R L, Walker R J, et al. 2011. Mapping lithospheric boundaries using Os isotopes of mantle xenoliths: An example from the North China Craton[J]. *Geochimica et Cosmochimica Acta*, 75(13): 3 881~3 902.
- Lynn K J, Garcia M O, Shea T, et al. 2017. Timescales of mixing and storage for Keanakāko‘i Tephra magmas ($1\ 500\sim 1\ 820^{\circ}\text{C}$), Kīlauea Volcano, Hawai‘i[J]. *Contributions to Mineralogy and Petrology*, 172(9): 1~20.
- Ma Jinlong and Xu Yigang. 2004. Petrology and geochemistry of the Cenozoic basalts from Yangyuan of Hebei Province and Datong of Shanxi province: Implications for the deep process in the western North China Craton[J]. *Geochimica*, 33(1): 75~88 (in Chinese with English abstract).
- Meng Q. 2003. What drove late Mesozoic extension of the northern China-Mongolia tract? [J]. *Tectonophysics*, 369(3~4): 155~174.
- Menzies M A, Fan W and Zhang M. 1993. Palaeozoic and Cenozoic lithoprobes and the loss of >120 km of Archaean lithosphere, Sino-Korean craton, China[J]. *Geological Society, London, Special Publications*, 76(1): 71~81.
- Mondal S K, Ripley E M, Li C, et al. 2006. The genesis of Archaean chromitites from the Nuasahi and Sukinda massifs in the Singhbhum Craton, India[J]. *Precambrian Research*, 148(1~2): 45~66.
- Moseley D. 1984. Symplectic exsolution in olivine[J]. *American Mineralogist*, 69(1~2): 139~153.
- Moussallam Y, Rose-Koga E F, Koga K T, et al. 2019. Fast ascent rate during the 2017~2018 Plinian eruption of Ambae (Aoba) volcano: A petrological investigation[J]. *Contributions to Mineralogy and Petrology*, 174(11): 1~24.
- Nekrylov N, Plechov P Y, Gritsenko Y D, et al. 2021. Major and trace element composition of olivine from magnesian skarns and silicate marbles[J]. *American Mineralogist*, 106(2): 206~215.
- Ozawa K. 1984. Olivine-spinel geospeedometry: Analysis of diffusion-controlled Mg-Fe²⁺ exchange[J]. *Geochimica et Cosmochimica Acta*,

- ta, 48(12): 2 597~2 611.
- O'Neill C and Spiegelman M. 2010. Formulations for simulating the multi-scale physics of magma ascent [A]. Dosseto A, Turner S and van Orman J. *Timescales of Magmatic Processes: From Core to Atmosphere* [C]. Chichester, UK: John Wiley & Sons, 87~101.
- O'Reilly S Y and Griffin W L. 2011. Rates of magma ascent: Constraints from mantle-derived xenoliths [A]. Dosseto A, Turner S and van Orman J. *Timescales of Magmatic Processes: From Core to Atmosphere* [C]. Chichester, UK: John Wiley & Sons, 116~124.
- Panina L I, Stoppa F and Usol'tseva L M. 2003. Genesis of melilitite rocks of Pian di Celle volcano, Umbrian kamafugite province, Italy: Evidence from melt inclusions in minerals [J]. *Petrology*, 11(4): 365~382.
- Pei Jingxian. 1981. Thermoluminescence ages of the volcanic flow-baked sediments in Datong area [J]. *Chinese Science Bulletin*, 26(16): 1 003~1 005 (in Chinese).
- Peslier A H and Luhr J F. 2006. Hydrogen loss from olivines in mantle xenoliths from Simcoe (USA) and Mexico: Mafic alkalic magma ascent rates and water budget of the sub-continental lithosphere [J]. *Earth and Planetary Science Letters*, 242(3~4): 302~319.
- Petrelli M and Zellmer G F. 2020. Rates and timescales of magma transfer, storage, emplacement, and eruption [J]. *Dynamic Magmatic Evolution*: 1~41.
- Pichavant M and Macdonald R. 2007. Crystallization of primitive basaltic magmas at crustal pressures and genesis of the calc-alkaline igneous suite: Experimental evidence from St Vincent, Lesser Antilles arc [J]. *Contributions to Mineralogy and Petrology*, 154(5): 535~558.
- Plechov P Y, Nekrylov N A, Shcherbakov V D, et al. 2017. Extreme-Mg olivines from venancite lavas of Pian di Celle volcano (Italy) [J]. *Doklady Earth Sciences*, 474(1): 507~510.
- Plechov P Y, Shcherbakov V D and Nekrylov N A. 2018. Extremely magnesian olivine in igneous rocks [J]. *Russian Geology and Geophysics*, 59(12): 1 702~1 717.
- Ray A, Hatui K, Paul D K, et al. 2016. Mantle xenolith-xenocryst-bearing monogenetic alkali basaltic lava field from Kutch Basin, Gujarat, Western India: Estimation of magma ascent rate [J]. *Journal of Volcanology and Geothermal Research*, 312: 40~52.
- Ren J, Tamaki K, Li S, et al. 2002. Late Mesozoic and Cenozoic rifting and its dynamic setting in Eastern China and adjacent areas [J]. *Tectonophysics*, 344(3~4): 175~205.
- Rivalta E, Taisne B, Burger A P, et al. 2015. A review of mechanical models of dike propagation: Schools of thought, results and future directions [J]. *Tectonophysics*, 638: 1~42.
- Rosatelli G, Stoppa F and Jones A P. 2000. Intrusive calcite-carbonatite occurrence from Mt. Vulture volcano, southern Italy [J]. *Mineralogical Magazine*, 64(4): 615~624.
- Ruprecht P and Plank T. 2013. Feeding andesitic eruptions with a high-speed connection from the mantle [J]. *Nature*, 500(7460): 68~72.
- Rutherford M J. 2008. Magma ascent rates [J]. *Reviews in Mineralogy and Geochemistry*, 69(1): 241~271.
- Sigurdsson H and Brown G M. 1970. An unusual enstatite-forsterite basalt from Kolbeinsey Island, North of Iceland [J]. *Journal of Petrology*, 11(2): 205~220.
- Sobolev A V, Hofmann A W, Kuzmin D V, et al. 2007. The amount of recycled crust in sources of mantle-derived melts [J]. *Science*, 316(5823): 412~417.
- Sobolev N V, Logvinova A M, Zedgenizov D A, et al. 2009. Petrogenetic significance of minor elements in olivines from diamonds and peridotite xenoliths from kimberlites of Yakutia [J]. *Lithos*, 112: 701~713.
- Sobolev N V, Sobolev A V, Tomilenko A A, et al. 2015. Paragenesis and complex zoning of olivine macrocrysts from unaltered kimberlite of the Udachnaya-East pipe, Yakutia: Relationship with the kimberlite formation conditions and evolution [J]. *Russian Geology and Geophysics*, 56(1~2): 260~279.
- Sparks R S J and Walker G P L. 1977. The significance of vitric-enriched air-fall ashes associated with crystal-enriched ignimbrites [J]. *Journal of Volcanology and Geothermal Research*, 2(4): 329~341.
- Spera F J. 1980. Aspects of magma transport [A]. Hargraves E B. *Physics of Magmatic Processes* [C]. Princeton N J: Princeton University Press, 265~323.
- Spera F J. 1984. Carbon dioxide in petrogenesis III: Role of volatiles in the ascent of alkaline magma with special reference to xenolith-bearing mafic lavas [J]. *Contributions to Mineralogy and Petrology*, 88(3): 217~232.
- Spera F J. 1987. Dynamics of translithospheric migration of metasomatic fluid and alkaline magma [A]. Menzies M A and Hawesworth. *Mantle Metasomatism* [C]. London: Academic Press, 1~20.
- Sun Jiaxiang, Li Ni and Zhang Wenqian. 2020. Petrogenesis and characteristics of the mantle source for the Quaternary Datong basalt: Research on the major, trace elements and Sr-Nd-Pb-Hf isotopes [J]. *Acta Petrologica Sinica*, 36(11): 3 331~3 345 (in Chinese with English abstract).
- Sundermeyer C, Di Muro A, Gordeychik B, et al. 2020. Timescales of magmatic processes during the eruptive cycle 2014~2015 at Piton de la Fournaise, La Réunion, obtained from Mg-Fe diffusion modelling in olivine [J]. *Contributions to Mineralogy and Petrology*, 175(1): 1~16.
- Szabó C S and Bodnar R J. 1996. Changing magma ascent rates in the Nőgrád-Gömör volcanic field Northern Hungary/Southern Slovakia: Evidence from CO₂-rich fluid inclusions in metasomatized upper man-

- tle xenoliths[J]. *Petrology*, 4(3): 221~230.
- Tang H, Matsumoto T, Zheng J, et al. 2014. Heterogeneous lithospheric mantle metasomatism in the eastern North China Craton: He-Ar isotopes in peridotite xenoliths from Cenozoic basalts[J]. *Journal of Asian Earth Sciences*, 80: 185~196.
- Tang Y J, Zhang H F, Nakamura E, et al. 2007. Lithium isotopic systematics of peridotite xenoliths from Hannuoba, North China Craton: Implications for melt-rock interaction in the considerably thinned lithospheric mantle [J]. *Geochimica et Cosmochimica Acta*, 71(17): 4 327~4 341.
- Treiman A H and Essene E J. 1984. A periclase-dolomite-calcite carbonatite from the Oka complex, Quebec, and its calculated volatile composition [J]. *Contributions to Mineralogy and Petrology*, 85(2): 149~157.
- Wan Yusheng, Liu Dunyi, Dong Chunyan, et al. 2009. The oldest rocks and zircons in China[J]. *Acta Petrologica Sinica*, 25(8): 1 793~1 807(in Chinese with English abstract).
- Wan Yusheng, Song Biao, Liu Dunyi, et al. 2001. Geochronology and geochemistry of 3.8~2.5 Ga ancient rock belt in the Dongshan scenic park, Anshan area[J]. *Acta Geologica Sinica*, 75(3): 363~370 (in Chinese with English abstract).
- Wan Yusheng, Song Biao, Yang Chun, et al. 2005. Zircon SHRIMP U-Pb Geochronology of Archean rocks from the Fushun-Qingyuan area, Liaoning Province and its geological significance [J]. *Acta Geologica Sinica*, 79(1): 78~87 (in Chinese with English abstract).
- Wanamaker B J, Bergman S C and Evans B. 1982. Crack healing in silicates: Observations on natural lherzolite nodules[J]. *Transactions of the American Geophysical Union*, 63: 437.
- Wanamaker B J, Wong T F and Evans B. 1990. Decrepitation and crack healing of fluid inclusions in San Carlos olivine[J]. *Journal of Geophysical Research: Solid Earth*, 95(B10): 15 623~15 641.
- Wang Nailiang, Yang Jingchun, Xia Zhengkai, et al. 1996. Shanxi Graben System, Cenozoic Sedimentary and Tectonic Geomorphology [M]. Beijing: Science Press(in Chinese).
- Wang T, Zheng Y, Zhang J, et al. 2011. Pattern and kinematic polarity of late Mesozoic extension in continental NE Asia: Perspectives from metamorphic core complexes[J]. *Tectonics*, 30(6): 1~27.
- Wenzel T, Baumgartner L P, Brügmann G E, et al. 2002. Partial melting and assimilation of dolomitic xenoliths by mafic magma: The Iok-Dovyren intrusion (North Baikal Region, Russia)[J]. *Journal of Petrology*, 43(11): 2 049~2 074.
- Wu F, Yang J, Xu Y, et al. 2019. Destruction of the North China craton in the Mesozoic[J]. *Annual Review of Earth and Planetary Sciences*, 47: 173~195.
- Wu F, Zhang Y, Yang J, et al. 2008. Zircon U-Pb and Hf isotopic constraints on the Early Archean crustal evolution in Anshan of the North China Craton[J]. *Precambrian Research*, 167(3~4): 339~362.
- Xiong F, Yang J, Robinson P T, et al. 2015. Origin of podiform chromite, a new model based on the Luobusa ophiolite, Tibet[J]. *Gondwana Research*, 27(2): 525~542.
- Xu W, Wang C, Yang D, et al. 2010a. Dunite xenoliths and olivine xenocrysts in gabbro from Taihang Mountains: Characteristics of Mesozoic lithospheric mantle in Central China[J]. *Journal of Earth Science*, 21(5): 692~710.
- Xu W, Yang D, Gao S, et al. 2010b. Geochemistry of peridotite xenoliths in Early Cretaceous high-Mg[#] diorites from the Central Orogenic Block of the North China Craton: The nature of Mesozoic lithospheric mantle and constraints on lithospheric thinning[J]. *Chemical Geology*, 270(1~4): 257~273.
- Xu X, Yang J, Chen S, et al. 2009. Unusual mantle mineral group from chromitite orebody Cr-11 in Luobusa ophiolite of Yarlung-Zangbo suture zone, Tibet[J]. *Journal of Earth Science*, 20(2): 284~302.
- Xu Y. 2002. Evidence for crustal components in the mantle and constraints on crustal recycling mechanisms: Pyroxenite xenoliths from Hannuoba, North China[J]. *Chemical Geology*, 182(2~4): 301~322.
- Xu Yigang. 2006. Formation of the Taihangshan gravity lineament by the diachronous lithospheric thinning of the North China Craton [J]. *Earth Science—Journal of China University of Geosciences*, 31(1): 14~22(in Chinese with English abstract).
- Xu Y, Ma J, Frey F A, et al. 2005. Role of lithosphere-asthenosphere interaction in the genesis of Quaternary alkali and tholeiitic basalts from Datong, western North China Craton[J]. *Chemical Geology*, 224(4): 247~271.
- Yao J, Zhang G, Wang S, et al. 2021. Recycling of carbon from the stagnant paleo-Pacific slab beneath Eastern China revealed by olivine geochemistry[J]. *Lithos*, 398~399: 106249.
- Yang J, Meng F, Xu X, et al. 2015. Diamonds, native elements and metal alloys from chromitites of the Ray-Iz ophiolite of the Polar Urals [J]. *Gondwana Research*, 27(2): 459~485.
- Ye H, Zhang B and Mao F. 1987. The Cenozoic tectonic evolution of the Great North China: Two types of rifting and crustal necking in the Great North China and their tectonic implications[J]. *Tectonophysics*, 133(3~4): 217~227.
- Zhai Mingguo. 2006. Geological significance of the Neoarchean global cratonization event and the boundary between Archean and Proterozoic [J]. *Geotectonica et Metallogenesis*, 30(4): 419~421 (in Chinese with English abstract).
- Zhai Mingguo. 2011. Cratonization and the Ancient North China Continent: A summary and review[J]. *Science China Earth Sciences*, 54(8): 1 110~1 120.
- Zhai M and Liu W. 2003. Palaeoproterozoic tectonic history of the North

- China craton: A review [J]. *Precambrian Research*, 122(1~4): 183~199.
- Zhang H, Huang Q, Zhao G, et al. 2016. Three-dimensional conductivity model of crust and uppermost mantle at the northern Trans North China Orogen: Evidence for a mantle source of Datong volcanoes [J]. *Earth and Planetary Science Letters*, 453: 182~192.
- Zhang H, Liu J, Santosh M, et al. 2017. Ultra-depleted peridotite xenoliths in the Northern Taihang Mountains: Implications for the nature of the lithospheric mantle beneath the North China Craton [J]. *Gondwana Research*, 48: 72~85.
- Zhang H, Sun M, Zhou X, et al. 2003. Secular evolution of the lithosphere beneath the eastern North China Craton: Evidence from Mesozoic basalts and high-Mg andesites [J]. *Geochimica et Cosmochimica Acta*, 67(22): 4 373~4 387.
- Zhang Shimin, Dou Suqin and Yang Jingchun. 1997. Characteristics of the Datong Quaternary volcano group [J]. *Bulletin of the Institute of Crustal Dynamics*, 11: 103~111 (in Chinese).
- Zhang S, Zhao Y, Davis G A, et al. 2014. Temporal and spatial variations of Mesozoic magmatism and deformation in the North China Craton: Implications for lithospheric thinning and decratonization [J]. *Earth-Science Reviews*, 131: 49~87.
- Zhang Yanbo. 1986. Characteristics of petrology of the Datong basalts [J]. *Seismology and Geology*, 8(1): 59~67 (in Chinese with English abstract).
- Zhang Yigang and E Molan. 1994. The oxygen fugacities of Cenozoic basaltic magmas and their enclosed mantle xenoliths [J]. *Acta Petrologica Sinica*, 10(2): 161~170 (in Chinese with English abstract).
- Zhao G, Sun M, Wilde S A, et al. 2003. Assembly, accretion and breakup of the Paleo-Mesoproterozoic Columbia Supercontinent: Records in the North China Craton [J]. *Gondwana Research*, 6(3): 417~434.
- Zhao G, Sun M, Wilde S A, et al. 2005. Late Archean to Paleoproterozoic evolution of the North China Craton: Key issues revisited [J]. *Precambrian Research*, 136(2): 177~202.
- Zhao G, Wilde S A, Cawood P A, et al. 1999. Thermal evolution of two textural types of mafic granulites in the North China craton: Evidence for both mantle plume and collisional tectonics [J]. *Geological Magazine*, 136(3): 223~240.
- Zhao G, Wilde S A, Cawood P A, et al. 2001. Archean blocks and their boundaries in the North China Craton: Lithological, geochemical, structural and *P-T* path constraints and tectonic evolution [J]. *Precambrian Research*, 107(1~2): 45~73.
- Zhao G, Wilde S A, Guo J, et al. 2010. Single zircon grains record two Paleoproterozoic collisional events in the North China Craton [J]. *Precambrian Research*, 177(3~4): 266~276.
- Zhao X M, Zhang H F, Zhu X K, et al. 2015. Effects of melt percolation on iron isotopic variation in peridotites from Yangyuan, North China Craton [J]. *Chemical Geology*, 401: 96~110.
- Zharikov V A. 1970. Skarns (part I) [J]. *International Geology Review*, 12(5): 541~559.
- ### 附中文参考文献
- 安卫平, 苏宗正. 2008. 山西大同火山地貌 [J]. *山西地震*, 1: 1~5.
- 陈玲. 2019. 山西大同新生代火山群碱性玄武岩喷发前状态研究 [D]. 北京: 中国地质大学(北京).
- 陈文寄, 李大明, 戴潼漠, 等. 1992. 大同第四纪玄武岩的K-Ar年龄及过剩氩 [A]. 刘若新. 中国新生代火山岩年代学与地球化学 [C]. 北京: 地震出版社, 81~92.
- 陈孝德, 史兰斌, 林传勇. 2001. 华北第四纪火山作用研究 [J]. *地震地质*, 23(4): 564~573.
- 樊祺诚, 陈文寄, Hurford A J, 等. 1992. 大同玄武岩主要元素和微量元素化学 [A]. 刘若新. 中国新生代火山岩年代学与地球化学 [C]. 北京: 地震出版社, 93~100.
- 李虎侯, 孙建中. 1984. 用热释光年龄研究大同火山活动的时代 [J]. *中国科学(B辑)*, 14(7): 637~644.
- 马金龙, 徐义刚. 2004. 河北阳原和山西大同新生代玄武岩的岩石地球化学特征: 华北克拉通西部深部地质过程初探 [J]. *地球化学*, 33(1): 75~88.
- 裴静娴. 1981. 大同地区火山岩流烘烤沉积物的热发光年龄测定 [J]. *科学通报*, 26(16): 1 003~1 005.
- 孙嘉祥, 李霓, 张雯倩. 2020. 大同第四纪玄武岩成因; 主微量元素及 Sr-Nd-Pb-Hf 同位素研究 [J]. *岩石学报*, 36(11): 3 331~3 345.
- 万渝生, 刘敦一, 董春艳, 等. 2009. 中国最老岩石和锆石 [J]. *岩石学报*, 25(8): 1 793~1 807.
- 万渝生, 宋彪, 刘敦一, 等. 2001. 鞍山东山风景区 3.8~2.5 Ga 古老岩带的同位素地质年代学和地球化学 [J]. *地质学报*, 75(3): 363~370.
- 万渝生, 宋彪, 杨淳, 等. 2005. 辽宁清原地区太古宙岩石 SHRIMP 锆石 U-Pb 年代学及其地质意义 [J]. *地质学报*, 79(1): 78~87.
- 王乃樑, 杨景春, 夏正楷, 等. 1996. 山西地堑系新生代沉积与构造地貌 [M]. 北京: 科学出版社.
- 徐义刚. 2006. 太行山重力梯度带的形成与华北岩石圈减薄的时空差异性有关 [J]. *地球科学*, 31(1): 14~22.
- 翟明国. 2006. 新太古代全球克拉通事件与太古宙-元古宙分界的地质涵义 [J]. *大地构造与成矿学*, 30(4): 419~421.
- 翟明国. 2011. 克拉通化与华北陆块的形成 [J]. *中国科学: 地球科学*, 41(8): 1 037~1 046.
- 张世民, 窦素芹, 杨景春. 1997. 大同第四纪火山群的活动特点 [J]. *地壳构造与地壳应力文集*, 11: 103~111.
- 张彦波. 1986. 大同地区玄武岩的岩石学特征 [J]. *地震地质*, 8(1): 59~67.
- 张毅刚, 鄂莫岗. 1994. 中国东部新生代玄武岩及其他地幔包体的氧逸度 [J]. *岩石学报*, 10(2): 161~170.